Seasonal variation in phosphorus concentration-discharge hysteresis inferred from high-frequency *in situ* monitoring

M.Z. Bieroza and A.L. Heathwaite

Lancaster Environment Centre, Lancaster University, Lancaster,

LA1 4YQ, UK

E-mail: m.bieroza@lancaster.ac.uk

ABSTRACT

High-resolution *in situ* total phosphorus (TP), total reactive phosphorus (TRP) and turbidity (TURB) time series are presented for a groundwater-dominated agricultural catchment. Meta-analysis of concentration-discharge (*c*-*q*) intra-storm signatures for 61 storm events revealed dominant hysteretic patterns with similar frequency of anti-clockwise and clockwise responses; different determinands (TP, TRP, TURB) behaved similarly. We found that the *c*-*q* loop direction is controlled by seasonally variable flow discharge and temperature whereas the magnitude is controlled by antecedent rainfall. Anti-clockwise storm events showed lower flow discharge and higher temperature compared to clockwise events. Hydrological controls were more important for clockwise events and TP and TURB responses, whereas in-stream biogeochemical controls were important for anti-clockwise storm events and TRP responses. Based on the best predictors of the direction of the hysteresis loops, we calibrated and validated a simple fuzzy logic inference model (FIS) to determine likely direction of the *c*-*q* responses. We show that seasonal and inter-storm succession in clockwise and anti-clockwise responses corroborates the transition in P transport from a chemostatic to an episodic regime.

Our work delivers new insights for the evidence base on the complexity of phosphorus dynamics. We show the critical value of high-frequency *in situ* observations in advancing understanding of freshwater biogeochemical processes.

Keywords: High-frequency *in situ* nutrient monitoring, phosphorus, turbidity, groundwater-fed rivers, hyporheic zone, fuzzy inference system

1. INTRODUCTION

The macronutrients nitrogen (N), phosphorus (P) and carbon (C) are key controls of biogeochemical processes in catchments. Manipulation of the N and P cycles in agricultural systems has elevated nutrient concentrations with consequent deterioration in aquatic ecosystem health and water quality (Basu *et al.*, 2011; Heathwaite, 2010; Vitousek *et al.*, 1997; Whitehead and Crossman, 2012). European Water Framework Directive requires comprehensive water quality assessments, and for England and Wales, these are based on long-term but low-frequency surveillance network maintained by the Environment Agency. Such monitoring programmes provide broad insights into long-term trends (Harris and Heathwaite, 2011; Howden *et al*., 2010) but do not provide knowledge of the biogeochemical and hydrological processes operating at time scales shorter than the sampling frequency (Bieroza *et al*., 2014; Halliday *et al*., 2012; Kirchner *et al*., 2004).

Recent advances in *in situ* analytical capability have enabled automated and high-frequency sampling in rivers at timescales beyond what was achievable even a decade ago (Jordan *et al*., 2005; Neal *et al*., 2012). This allows not only an assessment of stream chemical and hydrological dynamics, but also much more reliable estimates of chemical flux (Johnes, 2007; Jordan and Cassidy, 2011; Rozemeijer *et al*., 2010). To date, high-frequency sampling has revealed a far more complex behaviour than inferred from low-frequency sampling and biogeochemical model predictions, including fractal and self-organization properties, non-self-averaging behaviour, non-stationarity and non-linearity (Harris and Heathwaite, 2005; Jordan and Cassidy, 2011; Kirchner and Neal, 2013). High-frequency sampling captures a broad range of nutrient concentrations in response to varying stream discharge and biogeochemical processes and therefore reveals patterns of behaviour which have not been seen previously including concentration-discharge (*c*-*q*) hysteresis, diurnal cycling and non-storm transfers (Bende-Michl *et al*., 2013; Heffernan and Cohen, 2010; Jordan *et al*., 2007; Wade *et al*., 2012a). The *c*-*q* hysteresis is a term describing non-linear solute or particulate behaviour during storm event leading to a different rate of concentration change on the rising limb compared to the falling limb of the hydrograph and time lags between the peak values of the chemograph and hydrograph as in Figure 1a (Bowes *et al*., 2005; House and Warwick, 1998; McDiffett *et al*., 1989). Non-linear solute or particulate behaviour in freshwater systems is commonly described using *c*-*q* hysteresis (Bowes *et al*., 2005; Donn *et al*., 2012; Hornberger *et al*., 2001; Lawler *et al*., 2006) but relatively little is known about the processes controlling their development and their seasonal succession (Bende-Michl *et al*., 2013). Clockwise *c*-*q* hysteresis describes solute or particulate concentrations that increase with increasing discharge, with higher concentrations measured on the rising limb compared to the falling limb of the hydrograph (Figure 1b) as a result of rapid flushing and exhaustion of solutes or particulates from the within- or next to- channel sources (Bowes *et al.*, 2009; Creed *et al.*, 1996; Jordan *et al.*, 2007). Anti-clockwise *c*-*q* hysteresis (Figure 1c) is typically associated with a delayed solute or particulate delivery from distant upstream tributaries or deeper subsurface zones (Creed *et al.*, 1996; Donn *et al.*, 2012; Lawler *et al.*, 2006).

Figure 1

The main limitation of earlier studies of *c*-*q* responses is a relatively small number of storm events used to characterise hysteresis patterns (Granger *et al.*, 2010), insufficient sampling of the short duration rising limbs (Evans and Davies, 1998), and analysis of *c*-*q* patterns for different rivers (Butturini *et al.*, 2006; House and Warwick, 1998) and locations along the stream (Bowes *et al.*, 2005) precluding a direct comparison of temporal changes in the hydrochemical functioning of the stream. Previous studies analysing storm P dynamics concentrated on relatively highly polluted streams with significant contribution of P-rich sewage effluent discharges exhibiting negative concentration relationship with flow (dilution during storm events) (Bowes *et al.*, 2012; Jarvie *et al.*, 2002a; Neal *et al.*, 2010a). A small number of studies presented P *c*-*q* dynamics in relatively clean groundwater-fed rural rivers dominated by diffuse sources and showing a positive P concentration relationship with flow (Donn *et al.*, 2012; Wade *et al.*, 2012b).

Our work builds on previous studies aimed at quantifying hysteretic *c*-*q* responses and provides new insights into P and sediments *c*-*q* behaviour in groundwater-fed catchment subject to diffuse pollution including the importance and seasonal variation in hydrological and biogeochemical controls of P and sediments transfers and transport and supply limitation. Based on a two year high-frequency biogeochemical and hydrological dataset we evaluate some common patterns observed in the P and sediments *c*-*q* relationship: (1) predominant clockwise hysteretic behaviour for P fractions and sediments, (2) random temporal succession of hysteresis responses and (3) the dominant role of antecedent hydrological and meteorological conditions including the exhaustion effect in controlling hysteretic behaviour. We hypothesise that in groundwater-fed catchments the hysteretic P and sediments patterns are more complex compared to surface-dominated catchments due to the potential for solutes delivery along subsurface pathways and importance of hyporheic P and sediments stores. In particular, this paper evaluates the *c*-*q* relationship on inter-storm and intra-storm bases, evaluates the dominant hysteresis patterns in P and sediments behaviour and examines potential controls of hysteresis direction and magnitude including the role of antecedent hydrological and meteorological conditions using an hourly dataset spanning two years. In the process, the data are used to test the efficacy of a simple expert-system based on fuzzy logic inference to determine the direction of hysteresis loops based on simple hydrological and meteorological metrics, and to evaluate the applicability of conventional optimisation methods in describing hysteretic behaviour.

2. MATERIALS AND METHODS

2.1 STUDY SITE

Hydrological and biogeochemical measurements have been undertaken in the River Leith catchment (54 km^2) in Cumbria (UK) since May 2009 (National Grid Reference: NY 5875 2440, Supporting Figure A); here we focus on the period to July 2011. Intensive hydrogeomorphological research reported elsewhere (Kaser *et al*., 2009; Krause *et al*., 2013) shown the river is a zone of dynamic groundwater-surface water interactions with strong groundwater accretion. The Leith catchment is of mixed geology with Carboniferous Limestone (SW) and Penrith Permo-Triassic Sandstone (NE) overlain by glacial till deposits (BGS, 2010). Catchment land use is dominated by the improved grassland (61%) with a small proportions of woodland (16%), arable land (14%) and rough low-productivity grassland (7%) (LCM2007, 2011).

The monitoring site is located upstream of point source inputs from Cliburn village illustrated by weak negative relationships between conservative markers of sewage effluent, boron and sodium (Neal *et al.*, 2010a) and soluble reactive phosphorus (SRP) concentrations (Bieroza *et al*., 2014). Rainfall and stream discharge data were obtained from the Environment Agency

(EA) for England and Wales[1]. The average annual rainfall total (2004-2011) measured with a tipping bucket gauge for the Oasis Penrith rainfall station (2.5 km N from the *in situ* laboratory) was 957 mm (*S.D.* 269 mm) (EA, 2012b).

2.2 ANALYTICAL METHODS

An automated and telemetered nutrient laboratory powered by batteries and solar panels for *in situ* analysis of stream water samples was installed in 2009. A peristaltic pump system delivers unfiltered river water samples to a WaterWatch 2610 multiparameter meter (Partech, 2013) on an hourly basis. The WaterWatch meter records water temperature (ºC), dissolved oxygen (%), conductivity (µS cm^{-1}), pH and redox potential (mV) and turbidity (TURB measured in nephelometric turbidity units (NTU)). The latter measurement is commonly used as a proxy for suspended sediment dynamics (Minella *et al.*, 2008). The stream water is directed to a sample pot of two MicroMac C analysers (Systea, 2013) facilitating measurements of total phosphorus (TP) and total reactive phosphorus (TRP). Total phosphorus (TP) is an integrated measure of both dissolved forms of P (orthophosphate, polymeric and organic) and particulate forms (PP) (Jarvie *et al.*, 2002b). The TP analysis is based on the UV/persulphate/acid digestion at high temperature (~97°C) followed by a modified phosphomolybdenum blue method (Murphy and Riley, 1962). *In situ* TP analysis takes 50 minutes and has been optimised for analytical accuracy. *In situ* TRP analysis, based on the phosphomolybdenum blue method (Murphy and Riley, 1962), takes approximately 10 minutes and is measured on unfiltered samples equating to SRP plus a fraction of particulate P that is reactive to the phosphomolybdenum blue method reagents (Jarvie *et al.*, 2002b). Routine lab maintenance takes place on a fortnightly basis including running the reference

[1] The Environment Agency is an executive non-departmental public body responsible to the Secretary of State for Environment, Food and Rural Affairs (http://www.environment-agency.gov.uk/)

standard to check the accuracy of the calibration. Manual (grab) samples are collected weekly for checking the performance of the *in situ* analysers. A comparison of P *in situ* and laboratory-based concentrations shows a consistently higher error associated with *in situ* TP than TRP (-25.4% and -9.2%) determinations (Bieroza *et al*., 2014). Here, all statistical analyses have been performed on uncorrected P concentrations to avoid adding additional uncertainty to data as the main focus of the paper is the timing of P responses rather than calculation of absolute concentrations and loads.

Discharge data are measured at 15 min intervals by an automated Environment Agency gauging station (NY 5896 2444) located approximately 200 m downstream of the monitoring unit (Supporting Figure A) (EA, 2012a). The representativeness of the flow conditions in the study period (2009-2011) over a long-term discharge regime was tested (from January 2004). The data analysed in this study cover a full range of flow conditions from the 4th to the 99th percentile, with the median value corresponding to the 46th flow percentile. In this paper we analysed biogeochemical responses to storm flows for 61 selected storm events comprising 14.4% of the study period flow record (Figure 2). Three storm events exceeded the bankfull discharge stage of 1.87 m (storms 12, 16, 49) and thus the Q_{max} values for these events are uncertain. Completeness of the discharge data in the study period was 99%.

2.3 DATA ANALYSIS AND STATISTICAL METHODS

All storm event *c*-*q* TP, TRP and TURB responses were examined visually for the presence and direction of hysteretic loops (Supporting Table B). For each storm event *c*-*q* data were plotted as in Figure 1 and classified into three types of responses: clockwise (C; Figure 1b), anti-clockwise (A; Figure 1c and 1e) and no hysteresis (Nh; Figure 1d) when a linear or unclear *c*-*q* pattern was observed. Hysteretic response was affirmed by differences in nutrient concentrations between the rising and falling limbs leading to a *c*-*q* loop and the presence of a time lag between peak concentration and peak discharge. A negative time lag indicates a clockwise pattern (peak concentration leads peak discharge), a positive time lag indicates an anti-clockwise pattern (peak concentration lags peak discharge) and no time lag indicates no-hysteresis pattern. A *c*-*q* loop with no time lag between peak concentration and peak discharge was therefore classified as Nh but a "figure 8" type of hysteresis loop as in Figure 1e was classified as a hysteretic response with the direction depending on the succession of the peak concentration and peak discharge in time. The latter pattern occurs when the concentration (or discharge) on the rising limb takes values both higher and lower than those on the falling limb. To describe *c*-*q* responses for each storm event a set of hydrological and biogeochemical characteristics was collated (Table 1 and Supporting Tables A).

Hysteresis *c*-*q* loops were described in terms of the direction using rotational parameter ΔR (Equation *Eq.* 1 in Supporting Table A) and response factors p_{HW} (*Eq*. 2) and p_B (*Eq*. 3) and the magnitude using magnitude parameter ΔC (*Eq*. 4), magnitude factor h (*Eq*. 2) and the gradient constant g (*Eq*.3). The ΔR and ΔC parameters are simple statistical descriptors (Butturini *et al.*, 2006) and the p_{HW}, p_B, g, h parameters are optimised using two empirical methods (Bowes *et al*., 2005; House and Warwick, 1998) (Table 1).

To examine the controls of hysteresis direction and magnitude we have performed a comprehensive meta-analysis including 1) non-parametric analysis of variance of mean hydrological and biogeochemical properties between A, Nh and C groups of hysteretic responses (Kruskal-Wallis test for data that do not come from a standard normal distribution as determined with Kolmogorov-Smirnov test), 2) pairwise comparisons between hysteresis descriptors and the explanatory hydrological and biogeochemical metrics using Spearman's rank correlations and 3) a multivariate non-parametric method of canonical redundancy analysis (RDA) to analyse interactions of explanatory hydrological and biogeochemical variables with hysteresis descriptors (response variables).

Spearman's correlations *p*-values were corrected for multiple comparisons and with Monte Carlo 1000 permutations test for an alpha level of 0.05 (Groppe *et al.*, 2011; Manly, 2007). The RDA analysis with stepwise forward selection of parameters was performed following a procedure described in the literature (Legendre and Legendre, 1998; Legendre and Anderson, 1999). The results of the RDA were plotted on a biplot diagram showing the interactions between response and explanatory variables and samples (storm events). Finally, based on the results of the meta-analysis, a fuzzy inference system (FIS) was developed to provide a prediction of hysteresis direction based on the most significant biogeochemical and hydrological descriptors.

For all analyses a uniform significance level of 0.05 was used. All data processing and statistical analyses were carried out in Matlab version 7.11.0 (R2010b) with Statistics toolbox version 7.4 and Fuzzy logic toolbox version 2.2.12. Readily available online Matlab functions were used to calculate corrected Spearman's rank correlations (Groppe, 2012) and redundancy analysis (Johnes, 2011).

Table 1

3. RESULTS

Hydrological and biogeochemical conditions prior to and during the storm events were characterised using a number of metrics (Supporting Tables A, B and C). In total, 61 storm events of varying magnitude and duration were observed in the period selected for study (June 2009 – July 2011) and reported in this paper (Figure 1).

Figure 2

3.1 STORM EVENT HYDROLOGICAL CHARACTERISTICS

The storm events varied greatly in terms of the antecedent rainfall conditions (seven day antecedent rainfall API_7 0 to 60 mm, total rainfall $RAIN_{tot}$ 0 to 40 mm, baseflow discharge prior to storm event Q_0 0.1 to 24.1 m^{3}s^{-1}, rainfall duration $\Delta RAIN$ 12 to 107 hours), the duration of the rising hydrograph limb *RL* (2.5 to 75.3 hours) and magnitude of a storm event measured as mean Q_{mean} (0.1 to 37.8 m^{3}s^{-1}) and maximum Q_{max} (0.15 to 113.0 m^{3}s^{-1}) discharge, covering a wide spectrum of hydrological conditions.

Autumn storms dominated (*N* = 21) over summer, winter and spring events (*N* = 15, 14 and 11 respectively). The greatest differences in meteorological and hydrological characteristics were observed between autumn and winter ($RAIN_{tot}$ 10 and 4 mm and API_7 29 and 12 mm) and summer and winter storms (H_{mean} 0.68 and 1.08 m and Q_{mean} 1.2 and 8.2 m^{3}s^{-1}). Average rainfall intensity ($RAIN_{int\_mean}$) in the study period was 0.80 mm h^{-1} (*N* = 61, *S.D.* 0.60 mm h^{-1}) suggesting a predominance of low intensity (<1.0 mm h^{-1}, for 42 events) rainfall events, with 16 storm events of intermediate intensity and with the remaining 3 storm events of high intensity (≥2 mm h^{-1}).

Intermittent losses of biogeochemical data occurred as a result of equipment malfunctioning during freezing conditions and when site access was restricted by floodwaters (Figure 2). A statistical comparison between storm events with (*N* = 61) and without (*N* = 34) biochemical data revealed that the monitoring lab malfunctions were coincident with episodes of consecutive, high magnitude storm events in response to intensive and short in duration rainfall. The majority of the storms without biogeochemical data occurred in the late autumn – early winter period, with just 2 periods constituting 47% of the total number of missing data events (11 consecutive storm events between 16 November – 12 December 2009 and 5 consecutive storm events between 10 – 29 December 2010).

3.2 STORM EVENT BIOGEOCHEMICAL CHARACTERISTICS

Mean baseflow P and TURB concentrations at the *in situ* lab (for Q_{mean} = 0.29 m^{3}s^{-1}, N = 1694) were typically low: TP 36.6 µg l^{-1} (*S.D.* 29.2 µg l^{-1}), TRP 29.8 µg l^{-1} (*S.D.* 23.2 µg l^{-1}), TURB 1.11 NTU (*S.D.* 1.46 NTU) and indicative of diffuse agricultural sources (Rothwell *et al*., 2010). A comparison between *in situ* and laboratory-determined fractions showed that dissolved P fractions are the main constituents of TP (total dissolved phosphorus TDP 82%, TRP 71% and SRP 67%) and that *in situ* TRP comprises mainly the monomeric phosphate (PO_4-P) (Bieroza *et al*., 2014).

For all storm events consistent increases in TP, TRP and TURB concentrations were observed with discharge (concentration effect) but the magnitude of the increases varied greatly from storm to storm (Figure 2). Concentrations of P and TURB varied by two and stream discharge by five orders of magnitude in the study period. On a full dataset basis, the overall *c*-*q* relationship (Figure 2) is complex, nonlinear and non-stationary with a great amount of scatter and no apparent trend discernible. On a storm event basis, the *c*-*q* relationship is in the form of straight lines (power-law relationship) corresponding to rising and falling limbs, angled between 25-80 degrees in relation to the horizontal discharge axis. As the slopes of rising and falling limbs for each storm event were similar, a single slope value was determined for a storm event by finding the best linear fit between log(c) and log(q) (Supporting Table C). For all storm events, positive slopes (m) were observed which indicate concentration effect: mean m TP 1.0 (*S.D.* 1.2), TRP 0.7 (*S.D.* 1.0), TURB 1.0 (*S.D.* 0.7).

Based on hysteresis classification, out of the total of 61 storm events, 20% exhibited no or unclear hysteresis pattern (12 storm events for TP, 13 TRP and 13 TURB). Both the clockwise and anti-clockwise hysteretic behaviours were observed with similar frequency: clockwise hysteresis (21 TP, 21 TRP and 26 TURB) and anti-clockwise hysteresis (21 TP, 24

TRP and 20 TURB). The *c*-*q* patterns were consistent between determinands for the majority of the storm events (51 events, 82%). For 11 storm events the patterns were inconsistent between determinands due to short time lags (values close to 0), which may affect their classification.

Analysis of variance showed clear and significant differences in hydrological and biogeochemical properties between three groups of storm events (anti-clockwise, no hysteresis and clockwise) (Supporting Table D) with several parameters changing along the hysteresis gradient A-Nh-C. These patterns were consistent between the three determinands. Mean values of concentration (baseline C_0, mean C_{mean}, maximum concentration C_{max} and concentration magnitude ΔC) and storm event magnitude measures (Q_0, Q_{mean}, mean stream stage H_{mean}, Q_{max}, volume of discharge Q_{vol} and discharge magnitude ΔQ_t) were the lowest for anti-clockwise events and gradually increasing for no hysteresis and clockwise events (Figures 3bcd). The pairwise comparisons (Supporting Table E) showed that the best discriminations were between anti-clockwise and clockwise events with no hysteresis events showing intermediate properties.

Figure 3

Anti-clockwise storm events were typically shorter (*t*), with shorter *RL* and larger absolute time lags (on average 5.5 hours) compared to clockwise responses (time lags of 2.5 hours on average). Mean time lags were similar for TP and TRP (A: TP 5.5, TRP 5.9, C: TP -2.7, TRP -2.8 hours) whereas TURB time lags were consistently shorter for both anti-clockwise and clockwise storm events (A 5.0, C -2.1 hours). The effect of the antecedent rainfall conditions on the direction of the hysteresis was neither clear nor significant with $p > 0.05$ (Kruskal-Wallis test, H<6.1 , 2 d.f.; Supporting Table D) for all descriptors (storm event duration Δt,

$RAIN_{tot}$, API_7, $RAIN_{int\_mean}$, $RAIN_{int\_max}$, $\Delta RAIN$) with the exception of Q_0 which increased along the A-Nh-C sequence. A consistent pattern of higher $TEMPA_{mean}$, RAD_{mean}, $TEMPW_{mean}$, $COND_{mean}$, pH_{mean} for anti-clockwise compared to clockwise events was observed and highly significant (Figures 3ef). Anti-clockwise events showed, on average, 3.5-3.8°C higher $TEMPA_{mean}$ across determinands than clockwise events.

Differences in mean log(*c*)-log(*q*) slope values between three groups of hysteresis patterns were observed for P fractions with higher slopes for anti-clockwise events and lower slopes for clockwise events, however the differences were statistically significant only for TRP (Figure 3a and Supporting Tables D and E). Mean TP and TRP slope values varied on a seasonal basis with summer storm events showing higher slopes than during the rest of year (significant for TRP $p = 0.01$) and with similar slopes for consecutive storm events.

3.3 CONTROLS OF HYSTERESIS C-Q RESPONSES

The statistical significance of hydrological and biogeochemical variables in explaining *c*-*q* hysteresis patterns was tested with pairwise Spearman's correlations and a RDA analysis to provide information on the physical meaning of hysteresis descriptors (Tables 1 and 2 and Figure 4). Four hysteresis descriptors were tested (p_{HW}, h, ΔR and ΔC) as the p_B and g parameters were omitted due to large mean errors (Supporting Text A and Supporting Table F).

Table 2

Pairwise RDA correlations between hysteresis descriptors (response variables) and environmental parameters (explanatory variables) showed as expected a high degree of collinearity between elements of each group. The corresponding rotational and magnitude hysteresis descriptors were correlated: p_{HW} was correlated with ΔR and h was correlated with ΔC and showed similar strength correlations with hydrological and biogeochemical parameters. The rotational parameters (p_{HW} and ΔR) explained a much larger proportion of the total variance (first canonical axis explaining 81% TP, 72% TRP and 82% TURB of the variance) compared to the magnitude parameters h and ΔC (the second canonical axis explaining 10% TP, 9% TRP and 10% TURB of the total variance).

Figure 4

The parameters encompassing the information about the hysteresis direction (p_{HW} and ΔR) produced significant positive correlations with the discharge descriptors (Q_{max}, Q_{vol}, Q_{mean}, *Load* see *Eq*. 6 in Supporting Table A) and negative correlations with the thermal measures (RAD_{mean}, $TEMPA_{mean}$, $TEMPW_{mean}$) (Figure 4 and Supporting Table G). Partial RDA analysis showed that five explanatory variables yielded the largest proportion of the variance explained: Q_{vol} (TP 34%, TRP 15%, TURB 29%), DO_{mean} (TP 31%, TRP 22%, TURB 27%), pH_{mean} (TP 25%, TRP 20%, TURB 29%), $TEMPA_{mean}$ (TP 25%, TRP 26%, TURB 24%) and $TEMPW_{mean}$ (TP 25%, TRP 25%, TURB 24%) (Supporting Table G). The variance explained was similar for TP and TURB whereas TRP showed a weaker dependency on Q_{vol} and stronger on $TEMPA_{mean}$.

Both hysteresis magnitude parameters (h and ΔC) showed strong and significant correlations with the concentration measures (C_{max} and C_{mean}). Turbidity hysteresis magnitude descriptors were also positively correlated with the stream discharge measures (Q_{max}, Q_{vol}, Q_{mean}, *Load*). The effect of antecedent conditions was important for the magnitude of the hysteresis but not for the direction of the hysteresis. Rainfall characteristics (API_7, $RAIN_{tot}$, $RAIN_{int\_mean}$, $RAIN_{int\_max}$, $\Delta RAIN$) explained only a small proportion of the variance (<10%) in response variables for TP and TRP and moderate for TURB (<38%). Both positive (with $RAIN_{tot}$,$RAIN_{int\_mean}$, $RAIN_{int\_max}$) and negative (with API_7, Q_0) correlations were observed suggesting a complex relationship with antecedent rainfall patterns. No significant correlations were observed for the duration of rainfall ($\Delta RAIN$).

Three variables were shown to control the direction of *c*-*q* hysteresis patterns Q_{vol}, $TEMPW_{mean}$ and $TEMPA_{mean}$. As both temperature metrics show similar behaviour in explaining hysteresis patterns and there is a strong linear correlation between them ($TEMPW_{mean}$ = 0.63*$TEMPA_{mean}$ + 7.0, N=6620, Pearson's r = 0.92), we have solely used $TEMPA_{mean}$ for further analysis. Based on the observation that anti-clockwise responses are predominant for low Q_{vol} and high $TEMPA_{mean}$ and clockwise responses are typical for high Q_{vol} and low $TEMPA_{mean}$ a simple set of if-then rules (Table 3) and membership functions (Figure 5) were defined for the FIS.

Table 3

Figure 5

The FIS provided an indication of hysteresis direction for each storm event based on discharge volume and mean air temperature (Table 4). The closer the value of the degree of the output membership function to -1, the higher the probability of an anti-clockwise hysteresis, likewise the probability of a clockwise hysteresis increases for results closer to 1. The non-hysteresis responses were omitted in the model due to lack of significant differences in mean values of hydrological and biogeochemical variables compared to anti-clockwise and clockwise events (Supporting Table E). Thus, anti-clockwise responses were predicted for < 0 and clockwise for > 0 values of the output membership function (Figure 4c). The dataset was randomly divided into calibration (40 storm events) and validation data (21 storm events) and the FIS expert system provided a correct indication of hysteresis direction in 92.5% in the calibration step and 90.5% in the validation step. Only 5 storm events were misclassified (storm events 32, 33, 34, 37 and 57; Table 4).

Table 4

Finally, we provide a secondary validation of the FIS using the storm events when the *in situ* lab was not operational due to freezing and instruments malfunction. As the FIS for determination of hysteresis direction is based solely on hydrological and meteorological data, it was possible to test its performance on 34 storm events with missing or partially missing biogeochemical data. Out of 34 storm events, there was no biogeochemical data at all for 8 storm events. For the remaining 26 storm events the data were incomplete e.g. available for a single determinand or a part of the chemograph, making it possible to visually determine plausible hysteretic behaviour and contrast them with the FIS results. The direction of the *c*-*q* response was predicted correctly in 23 cases (88.5%), leaving only 3 storm events with incorrect classification. Of the correctly classified storm events, 74% of the responses were classified as clockwise and 26% as anti-clockwise, which is as expected based on the fact that the majority of the missing data occurred for storms in the late autumn-winter period (thus low $TEMPA_{mean}$ and high Q_{vol}).

4. DISCUSSION

4.1 HYSTERESIS PATTERNS

High-frequency water quality monitoring facilitates identification of intra-storm *c*-*q* dynamics and reveals patterns not previously observed using routine low-frequency and low-intensity sampling (Bieroza *et al*., 2014; Halliday *et al*., 2012; Jordan *et al*., 2007; Kirchner *et* *al*., 2004; Kirchner and Neal, 2013; Neal *et al*., 2012; Wade *et al*., 2012a). Below we evaluate P and turbidity (used as a proxy for fine sediments) *c-q* patterns revealed by the high frequency data in our study and contrast them with the patterns commonly observed in literature.

Firstly, we observed consistent increases in P (TP and TRP) and turbidity concentrations with stream discharge showing the predominance of concentration over the dilution effect and indicating that the nutrient and sediments delivery in the catchment is mainly controlled by diffuse pollution (Bieroza *et al*., 2014; Bowes *et al*., 2008; Neal *et al*., 2010b). We observed a lack of *c-q* correlation on a whole-dataset basis; however, for individual storm events and parts of the hydrograph the *c-q* relationships were strong as indicated by significant power-law fits. Similar *c-q* patterns for turbidity were observed by Walling and Webb (1982), which they linked with temporally dynamic sediment availability and flushing potential in the catchment. Recently complex patterns in high-frequency nutrient *c-q* responses were linked to the storm-to-storm dynamics of the critical source areas (CSAs) (Donn *et al.*, 2012; Thompson *et al.*, 2012) in surface-dominated catchments. In groundwater-dominated catchments mobile forms of P may be delivered along near subsurface flow pathways (Heathwaite and Dils, 2000; Mellander *et al*., 2012). The delivery of soluble P can therefore be delayed in time and distant in space from the source areas and P can potentially undergo substantial transformations (biological uptake, sorption to sediments) in soils, subsurface and in the hyporheic zone. These processes add to the complexity of *c-q* patterns in groundwater-dominated catchments that may reflect the temporally varying availability of P and sediments, the dynamic role of hydrological forcing on the rate of their delivery and delayed delivery along the subsurface pathways (Bende-Michl *et al.*, 2013; Donn *et al.*, 2012; Jordan *et al.*, 2005; Wade *et al.*, 2012b).

Secondly, we showed that the importance of hydrological forcing varied between storm events with lower, near-zero *c*-*q* slopes in log scale for clockwise loops and higher, above unity slopes for anti-clockwise storm events. Thus, clockwise events demonstrate stronger hydrological forcing relative to anti-clockwise events as near-zero slopes have been shown to corroborate chemostatic behaviour (Basu *et al.*, 2010; Thompson *et al.*, 2011). Basu *et al.* (2011) showed that P export follows two main regimes, chemostatic with low variability in concentration and episodic with high variability in concentration. Chemostatic P responses indicate transport limitation and the presence of large chemical sources that buffer variability in discharge concentrations so that the rate of P mobilisation is proportional to water flux (Basu *et al.*, 2011; Thompson *et al.*, 2011). Episodic behaviour indicates supply limitation and the presence of limited chemical stores in which case the rate of P mobilisation depends on the water flux and the P availability (Basu *et al.*, 2011; Thompson *et al.*, 2011). Chemostatic P export regime dominates for larger scales and heavily impacted catchments whereas episodic regime is typical for smaller spatial scales and pristine catchments (Basu *et al.*, 2011; Thompson *et al.*, 2011). Similar contribution of P clockwise and anti-clockwise patterns with flow observed in our study suggests that in groundwater-fed catchments both forms of P transport regime may be present. Our data suggest that the switch from a chemostatic regime, typified by clockwise responses, to an episodic regime typified by anti-clockwise responses is highly dynamic. It appears that this dynamic response is dependent on storm characteristics rather than being simply based on catchment characteristics as shown by previous research (Basu *et al.*, 2011; Thompson *et al.*, 2011). The clockwise responses are indicative of chemostatic behaviour and transport limitation presumably because near- and within-stream P and sediments sources are rapidly mobilised in response to hydrological forcing. For the anti-clockwise responses the role of direct hydrological forcing is subdued by a delayed subsurface delivery leading to a relative supply limitation.

Thirdly, we observed similar contributions of anti-clockwise and clockwise events and a high degree (82%) of consistency in the directional patterns between analysed determinands (TP, TRP, TURB). As shown in the literature, stream P *c*-*q* dynamics are dominated by clockwise patterns (Bowes *et al.*, 2005; Donn *et al.*, 2012; House and Warwick, 1998) and typically soluble and particulate P fractions show different intra-storm dynamics (Gburek *et al.*, 2005; Heathwaite and Dils, 2000). For example Bowes *et al.* (2005) observed anti-clockwise responses for P (SRP) for 35% of 10 storm events and consistent direction of the hysteresis loops between TP, SRP and PP for 41% of storm events. Hysteretic patterns in hydrological responses of in-stream solutes and particulates are often used to discriminate between different sources e.g. in-channel and distal catchment sources (Chanat *et al.*, 2002; Evans and Davies, 1998). Different typical delivery pathways of soluble P (delayed subsurface flow) and fine sediments and sediment-bound PP (rapid overland flow and within-stream mobilisation) (Donn *et al.*, 2012; Rozemeijer *et al.*, 2010) suggest that inconsistent hysteresis patterns for dissolved and particulate fractions should be expected. Gburek *et al.* (2005) showed that during a storm event turbidity peaks before TP as a result of mobilisation of PP with sediments and the SRP peak is lagged compared to TP due to delayed leaching from the soil in solution, a pattern that is not observed here. By contrast, we observed similar storm dynamics for all three determinands analysed in our study indicating similar behaviour for solutes and particulates. One explanation for consistent hysteretic behaviour of TP and TRP fractions is a large proportion of dissolved fraction in TP (on average 82%) and low particulate P content as indicated by previous laboratory tests (Bieroza *et al*., 2014). Consistent hysteresis patterns between TP (here predominantly in dissolved form) and TURB (a proxy for suspended sediments and sediment-bound PP) are more difficult to explain and suggest that delivery of P and fine sediments occurs along similar pathways and/or there is a similar source of soluble P and sediments on a storm event basis (Bende-Michl *et al.*, 2013).

Clockwise *c*-*q* behaviour of fine sediments is commonly linked with the depletion of the store of available sediments or increased contributions of subsurface flow during the falling limb of a hydrograph (Naden, 2010; Walling and Webb, 1982). A pre-event accumulation of sediments within the channel creates a transient source that is activated by the arrival of the wavefront (Bull, 1997). Rapid mobilisation of bed material, bank erosion and contribution from sources close to the stream have been shown to cause the rapid increase in sediments and P concentrations leading to clockwise *c*-*q* behaviour (Bowes *et al.*, 2005; Jarvie *et al.*, 2005; Jordan *et al.*, 2007; Palmer-Felgate *et al.*, 2009).

Anti-clockwise TRP responses have been linked to P transfers along shallow subsurface pathways (Donn *et al.*, 2012). However, the anti-clockwise *c*-*q* behaviour is unusual for turbidity and fine sediments as typically a limited supply of readily available sediments is flushed ("first flush" phenomena) during the rising hydrograph limb producing clockwise responses to discharge (Naden, 2010). Intermittent anti-clockwise turbidity responses can be linked to: (1) the exhaustion of local bed sediment stores and delayed delivery from distal sediment sources e.g. tributary streams, (2) biofilm break-up and/or in-stream sediment resuspension induced by progressive shear stress prior to and during the discharge peak and subsequent release of sediments later in the hydrograph and (3) the removal of a protective layer of superficial, readily entrained sediments and exposure of deeper layers of more consolidated fine sediments in subsequent small floods (Harvey *et al.*, 2012; Lawler *et al.*, 2006; Naden, 2010; Petticrew *et al.*, 2007; Wade *et al.*, 2012b). Donn *et al*. (2012) showed however that the first mechanism is less likely to explain anti-clockwise responses in lowland groundwater-fed parts of the catchment and stressed the role of subsurface delivery pathways. As our study reach is subject to intensive surface-groundwater interactions (Kaser *et al*., 2009; Krause *et al*., 2013), there is a large potential for solute delivery along hyporheic flow pathways, and occurrence of the second and the third mechanism, but this has not been investigated here. We did find that TURB showed hysteresis patterns similar to both P fractions but consistently shorter time lags to peak discharge for both clockwise and anti-clockwise responses. This may be due to rapid entrainment of fine sediments from predominant superficial storage in the bed and longer storage of solutes due to the expansion of hyporheic flow paths (Harvey *et al.*, 2012).

Fourthly, the role of antecedent conditions on the hysteresis direction and the magnitude of nutrient and sediment transfers has also been emphasised by previous studies (Bowes *et al.*, 2005; McDiffett *et al.*, 1989; Thompson *et al.*, 2012; Walling and Webb, 1982). The recovery period (Δt) is the time elapsed since a preceding storm and during which physical and biological processes operate to increase the store of available nutrients and sediments (Walling and Webb, 1982). Prolonged dry periods can be expected to result in an accumulation of P and sediments within the channel. Thus, the first storm after a dry period can result in rapid flushing of accumulated sediment material and high P and sediments concentrations (Bende-Michl *et al.*, 2013; Bowes *et al.*, 2005; McDiffett *et al.*, 1989). More frequent and intense rainfall events can result in depletion of the local P stores and lower in-stream concentrations (Wade *et al.*, 2012b). As expected in a groundwater-fed catchment the role of antecedent conditions in explaining the hysteresis patterns was complex and equivocal. The recovery time showed little and inconsistent impact on the magnitude of hysteretic patterns measured as a relative increase in concentration. High magnitude nutrient transfers were observed for relatively low magnitude storm events with short recovery times suggesting that in-stream sediment and nutrient sources are potentially more important in delivery than distant contributing areas of the catchment (Bende-Michl *et al.*, 2013; Donn *et al.*, 2012). Bowes *et al.* (2005) showed that the effect of in-stream and catchment P sources on the hysteretic patterns can be elucidated from the two optimisation parameters on a storm basis. They showed that the response parameter *pB* accounts for reactions of P with sediments and the gradient factor *g* accounts for the magnitude of the storm event and P mobilisation from the near-channel sources and more distant areas of the catchment. In our study (Supporting Text A) this optimisation method showed large errors between observed and optimised P and TURB concentrations and no significant correlations of the gradient factor *g* and the magnitude of the storm events were observed. The poor performance of the method is likely related to complex hysteretic patterns observed in our study as they rarely follow a simple loop pattern and often exhibit several concentration peaks and different behaviours at different stages of the hydrograph (Figure 1). This complex behaviour is likely correlated with multiple delivery flow pathways and hyporheic impacts observed in our groundwater-fed study catchment. A similar observation has been also made by Bowes *et al.* (2005) who suggested that their optimisation approach is prone to produce higher errors if the hysteresis patterns do not follow a simple loop pattern.

We also observed an effect of exhaustion of available P and sediment stores (supply limitation) during a succession of storm events similar to other studies (Bende-Michl *et al.*, 2013; Bowes *et al.*, 2005). From 15 storm sequences selected comprising from 2 to 5 storms (storms separated by less than 96 hours) flow-weighted concentrations for the majority showed consistent and significant ($p < 0.05$) decreasing trends (TP 9, TRP 11, TURB 10). However, contrary to observations made by other studies (Bowes *et al.*, 2005; Jordan *et al.*, 2005) the exhaustion effect was not controlling the direction of hysteresis loops (clockwise direction of the first storm event in series and anti-clockwise for the later events) which is in agreement with results presented by Siwek *et al.* (2012).

4.2 CONTROLS ON THE DIRECTION OF HYSTERESIS PATTERNS

We showed that the hysteresis direction was best explained by discharge volume and mean air/water temperature during the storm event and none of the rainfall characteristics were good discriminants. Discharge volume integrates the information on the magnitude and duration of a storm event and therefore characterises the intra-storm potential for bed sediments entrainment and effectiveness and the depth of sediment scouring (Bull, 1997). During large Q_{vol} events the potential erosion power is significant and may lead to rapid mobilisation of in-stream and near-stream sediment and nutrient stores leading to clockwise responses (Bowes *et al.*, 2005; Jordan *et al.*, 2007). Minor storm events with low Q_{vol}, low magnitude and short duration do not present enough shear stress and advective power (Bende-Michl *et al.*, 2013) to mobilise bed sediments and flush P accumulated in the hyporheic transient storage (Harvey *et al.*, 2012; Petticrew *et al.*, 2007).

Temperature controls both the rate of biological activity (e.g. microbial uptake, biofilm development on more stable gravels and boulders) and the rates of physico-chemical processes occurring at the surface-groundwater interface of the hyporheic zone including adsorption-desorption and precipitation-dissolution reactions (McDaniel *et al.*, 2009; Mulholland, 1992; Palmer-Felgate *et al.*, 2008; Stutter and Lumsdon, 2008). We found that temperature was a more important predictor of hysteresis direction for TRP compared to Q_{vol} which suggests less important role of hydrological forcing compared to temperature-controlled biochemical processes on in-stream fate and transfer of soluble P. Our results corroborate the findings of Rozemeijer *et al.* (2010) who argued that seasonality in temperature can explain some of the variability in P storm event responses not captured by hydrological characteristics.

We show based on high-frequency data that there is a seasonal behaviour (Figure 6) embedded in longer term nutrient behaviour e.g. 1/f scaling (Kirchner and Neal, 2013). As both temperature and discharge change seasonally (the majority of large storm events occurring in late autumn and winter), we argue that the direction of hysteresis loops undergoes seasonal succession and is predictable, with higher probability of anti-clockwise events in summer and higher probability of clockwise events in late autumn and winter (Table 4 and Figure 6). These findings contradict the results of Butturini *et al.* (2008) who suggested a random succession of different *c*-*q* responses as a result of complex effect of hydrological variables on the direction of the hysteretic loops.

The seasonal succession of anti-clockwise and clockwise events most likely reflects seasonal changes in hydrological conditions and effects of plant growth, nutrient uptake, release, mobilisation and delivery in the catchment (Bende-Michl *et al.*, 2013; Granger *et al.*, 2010; Heffernan and Cohen, 2010). We show that there is a seasonal transition between the two types of P transport regimes chemostatic typified by clockwise responses and episodic typified by anti-clockwise responses. In summer due to low hydrological forcing the nutrient delivery is dominated by low-energy subsurface pathways and mobilisation of the in-stream particulate sources delivered in the prior high flow periods (Bende-Michl *et al.*, 2013). Predominant subsurface delivery, in-stream sediments resuspension and chemical and biological solubilisation (Granger *et al.*, 2010; Jarvie *et al.*, 2005; Palmer-Felgate *et al.*, 2009) increase the probability of anti-clockwise hysteretic responses (89% in our study; Table 4) to low-magnitude storm events. Limited P and sediments availability indicates that the episodic P transfers and supply limitation dominate (Basu *et al.*, 2011). In winter with reduced plant cover and prolonged rainfall events the flow is dominated by flashier surface flows leading to rapidly established connectivity between nutrient sources and the stream network (Bende-Michl *et al.*, 2013; Bowes *et al.*, 2005; Donn *et al.*, 2012; Granger *et al.*, 2010) and predominant clockwise *c*-*q* behaviours (75% in our study; Table 4). Large P and sediment stores accumulated within and near the stream during summer are gradually mobilised during winter storms leading to chemostatic behaviour (Basu *et al.*, 2011) and clockwise *c*-*q* responses. Additional studies from other temperate agricultural catchments are required to fully validate our conceptual model of seasonal effects on P delivery and it is likely these responses are catchment-specific. For example, a study by Scott *et al*. (2001) shows that mineralisation of agricultural legacy P stores can lead to summer in-stream P concentrations maxima.

The clear seasonal pattern in hysteretic responses is corroborated by the fuzzy inference model which correctly explained the hysteresis direction for the majority of the storm events (calibration 93.3%, first validation 90.5% and second validation 88.5%). The model failed to correctly classify a number of low-magnitude, clockwise storm events (32-37) with high P and sediments transfers. These early autumn storm events coincided with an onset of lower ambient temperatures and followed a dry summer which potentially led to a significant accumulation of nutrient and sediments in within- and near-stream stores (Bende-Michl *et al.*, 2013; Jarvie *et al.*, 2005; Oeurng *et al.*, 2010). Several authors (Bende-Michl *et al.*, 2013; Bowes *et al.*, 2009; Evans *et al.*, 2004) have shown that due to transport limitation, flushing of these readily available nutrient sources in the beginning of the high flow period resulted in the highest annual TP and TRP concentrations and clockwise *c-q* behaviour. In addition, Bowes *et al.* (2009) showed that sudden cold weather could cause algal biofilms detachment from the substrate and sudden increases in the amount of readily available P-material not related to the occurrence or magnitude of a storm event. As the P and sediment transfers driven by transport limitation or biofilm break-up are incidental to seasonal temperature and discharge patterns, this atypical behaviour was not explained correctly by the FIS model.

5. CONCLUSIONS

We show that seasonally variable hydrological and biochemical factors control the *c-q* behaviour during storm events resulting in a seasonal transition between the chemostatic regime typified by clockwise responses and the dominance of hydrological forcing during winter and the episodic regime typified by anti-clockwise responses and lower hydrological forcing during summer. We note that this strong seasonal pattern was not observed for the first flush autumn events following long dry summers, which may be the result of within-stream accumulation of sediment-associated P.

We found that *c*-*q* responses varied between storm events and that the hysteretic responses were the dominant behaviour in P and sediments responses to increased river discharge. The clockwise and anti-clockwise events demonstrated similar occurrence frequency and consistency for all determinands (TP, TRP and TURB) throughout the study period. This suggests alignment P and fine sediment delivery pathways for this groundwater-fed system that is in contrast to surface-water catchments. Another contrasting observation was that the antecedent rainfall conditions and the exhaustion effect were poor predictors of the hysteresis direction and two seasonally-changing variables, discharge volume and air temperature explained the majority of the variance in the hysteretic responses. The clockwise responses were driven by hydrological forcing and may be linked to exhaustion of within-channel fine sediment and P sources. Anti-clockwise loops on the other hand resulted from delayed delivery of P and fine bed sediments.

Our results show the importance of the timing and frequency of collection of hydrochemical data for water quality monitoring and modelling in order to understand reach-scale nutrient dynamics. Hysteretic *c*-*q* responses can introduce a large uncertainty in the calculation of loads from instantaneous coarsely sampled flow and concentration data as substantial and variable time lags between peak flow and peak concentrations exist for different types of storm events (anti-clockwise, no hysteresis, clockwise) and determinands (TP, TRP, TURB). The results presented in this paper also have implications for catchment-scale sediment and nutrient modelling approaches aimed at predicting the risk of diffuse pollution and evaluation of the diffuse pollution mitigation measures. In groundwater-dominated catchments the subsurface and hyporheic delivery pathways may be important in controlling P and sediments fluxes as surface catchment drivers. Further investigation is needed to understand the role of subsurface and hyporheic impacts during lower magnitude storm events and their associated P and sediment sources. To meet the statutory requirements and advance our understanding of the complex *c*-*q* in-stream coupling in groundwater-fed catchments, further research is required to explain the role of transient hyporheic stores in modifying and propagating catchment sediment and nutrient fluxes. Additional lines of evidence are needed from detailed hydrogeological studies (Allen *et al*., 2014), combined with hydrograph separation approaches (Mellander *et al*., 2012) and tracer experiments (Baily *et al*., 2011) to infer potential delivery pathways and travel times from source to receptor.

ACKNOWLEDGMENTS

This work is supported by the Natural Environment Research Council NE/G001707/1 awarded to ALH. The authors would like to thank: Paddy Keenan for leading the laboratory analyses and *in situ* laboratory maintenance, Neil Mullinger for initiating the *in situ* lab programme; Heather Carter, Gareth McShane and a group of enthusiastic students from Lancaster Environment Centre (Mark Cooper, Tamara Kolbe, Chris Rowland) for helping with the lab and field work. Finally, a special thank you to Professors Colin Neal and Graham Harris for their invaluable feedback on the previous versions of this manuscript.

REFERENCES

Allen, D., Darling, W., Davies, J., Newell, A., 2014. Groundwater conceptual models: implications for evaluating diffuse pollution mitigation measures. Quarterly Journal of Engineering Geology and Hydrogeology, 47(1): 65-80.

Baily, A., Rock, L., Watson, C.J., Fenton, O., 2011. Spatial and temporal variations in groundwater nitrate at an intensive dairy farm in south-east Ireland: Insights from stable isotope data. Agriculture, Ecosystems & Environment, 144(1): 308-318.

Basu, N.B. et al., 2010. Nutrient loads exported from managed catchments reveal emergent biogeochemical stationarity. Geophysical Research Letters, 37.

Basu, N.B., Thompson, S.E., Rao, P.S.C., 2011. Hydrologic and biogeochemical functioning of intensively managed catchments: A synthesis of top-down analyses. Water Resources Research, 47(10): W00J15.

Bende-Michl, U., Verburg, K., Cresswell, H., 2013. High-frequency nutrient monitoring to infer seasonal patterns in catchment source availability, mobilisation and delivery. Environmental Monitoring and Assessment, 185(11): 9191-9219.

BGS, 2010. Bedrock geology UK, North - United Kingdom Geological Maps. British Geological Survey.

Bieroza, M.Z., Heathwaite, A.L., Mullinger, N.J., Keenan, P.O., 2014. Understanding nutrient biogeochemistry in agricultural catchments: the challenge of appropriate monitoring frequencies. Environmental Science: Processes & Impacts, 16(7): 1676-1691.

Bowes, M., House, W., Hodgkinson, R., Leach, D., 2005. Phosphorus-discharge hysteresis during storm events along a river catchment: the River Swale, UK. Water Research: 751-762.

Bowes, M., Smith, J., Jarvie, H., Neal, C., 2008. Modelling of phosphorus inputs to rivers from diffuse and point sources. Science of the Total Environment: 125-138.

Bowes, M., Smith, J., Neal, C., 2009. The value of high-resolution nutrient monitoring: A case study of the River Frome, Dorset, UK. Journal of Hydrology: 82-96.

Bowes, M.J. et al., 2012. High-frequency phosphorus monitoring of the River Kennet, UK: are ecological problems due to intermittent sewage treatment works failures? Journal of Environmental Monitoring, 14(12): 3137-3145.

Bull, L.J., 1997. Relative velocities of discharge and sediment waves for the River Severn, UK. Hydrological Sciences Journal-Journal Des Sciences Hydrologiques, 42(5): 649-660.

Butturini, A., Alvarez, M., Bernal, S., Vazquez, E., Sabater, F., 2008. Diversity and temporal sequences of forms of DOC and NO3-discharge responses in an intermittent stream: Predictable or random succession? Journal of Geophysical Research-Biogeosciences, 113(G3).

Butturini, A., Gallart, F., Latron, J., Vazquez, E., Sabater, F., 2006. Cross-site comparison of variability of DOC and nitrate c-q hysteresis during the autumn-winter period in three Mediterranean headwater streams: A synthetic approach. Biogeochemistry, 77(3).

Chanat, J.G., Rice, K.C., Hornberger, G.M., 2002. Consistency of patterns in concentration-discharge plots. Water Resources Research, 38(8): 10.

Creed, I.F. et al., 1996. Regulation of nitrate-N release from temperate forests: A test of the N flushing hypothesis. Water Resources Research, 32(11): 3337-3354.

Donn, M.J., Barron, O.V., Barr, A.D., 2012. Identification of phosphorus export from low-runoff yielding areas using combined application of high frequency water quality data and MODHMS modelling. Science of The Total Environment, 426(0): 264-271.

EA, 2012a. Cliburn (station number 760280) 15 minutes stage and stream discharge data.

EA, 2012b. Oasis Penrith (station number 601068) 15 minutes rainfall data.

Evans, C., Davies, T.D., 1998. Causes of concentration/discharge hysteresis and its potential as a tool for analysis of episode hydrochemistry. Water Resources Research, 34(1): 129-137.

Evans, D.J., Johnes, P.J., Lawrence, D.S., 2004. Physico-chemical controls on phosphorus cycling in two lowland streams. Part 2 - The sediment phase. Science of the Total Environment, 329(1-3): 165-182.

Gburek, W., Barberis, W., Haygarth, P., Kronvang, B., Stamm, C., 2005. Phosphorus mobility in the landscape. In: Sims, J., Sharpley, A. (Eds.), Phosphorus: agriculture and the environment. American Society of Agronomy, Madison, pp. 941-979.

Granger, S.J. et al., 2010. High Temporal Resolution Monitoring of Multiple Pollutant Responses in Drainage from an Intensively Managed Grassland Catchment Caused by a Summer Storm. Water Air and Soil Pollution, 205(1-4): 377-393.

Groppe, D., 2012. Correlation permutation test with correction for multiple comparisons

Groppe, D.M., Urbach, T.P., Kutas, M., 2011. Mass univariate analysis of event-related brain potentials/fields I: A critical tutorial review. Psychophysiology, 48(12): 1711-1725.

Halliday, S.J. et al., 2012. An analysis of long-term trends, seasonality and short-term dynamics in water quality data from Plynlimon, Wales. Science of the Total Environment, 434: 186-200.

Harris, G., Heathwaite, A., 2005. Inadmissible evidence: knowledge and prediction in land and riverscapes. Journal of Hydrology: 3-19.

Harris, G.P., Heathwaite, A.L., 2011. Why is achieving good ecological outcomes in rivers so difficult? Freshwater Biology, 57: 91-107.

Harvey, J.W. et al., 2012. Hydrogeomorphology of the hyporheic zone: Stream solute and fine particle interactions with a dynamic streambed. Journal of Geophysical Research-Biogeosciences, 117.

Heathwaite, A., 2010. Multiple stressors on water availability at global to catchment scales: understanding human impact on nutrient cycles to protect water quality and water availability in the long term. Freshwater Biology: 241-257.

Heathwaite, A.L., Dils, R.M., 2000. Characterising phosphorus loss in surface and subsurface hydrological pathways. Science of the Total Environment, 251: 523-538.

Heffernan, J.B., Cohen, M.J., 2010. Direct and indirect coupling of primary production and diel nitrate dynamics in a subtropical spring-fed river. Limnology and Oceanography, 55(2): 677-688.

Hornberger, G.M., Scanlon, T.M., Raffensperger, J.P., 2001. Modelling transport of dissolved silica in a forested headwater catchment: the effect of hydrological and chemical time scales on hysteresis in the concentration-discharge relationship. Hydrological Processes, 15(10): 2029-2038.

House, W.A., Warwick, M.S., 1998. Hysteresis of the solute concentration/discharge relationship in rivers during storms. Water Research, 32(8): 2279-2290.

Howden, N.J.K., Burt, T.P., Worrall, F., Whelan, M.J., Bieroza, M., 2010. Nitrate concentrations and fluxes in the River Thames over 140 years (1868-2008): are increases irreversible? Hydrological Processes, 24(18): 2657-2662.

Jarvie, H.P. et al., 2005. Role of river bed sediments as sources and sinks of phosphorus across two major eutrophic UK river basins: the Hampshire Avon and Herefordshire Wye. Journal of Hydrology, 304(1–4): 51-74.

Jarvie, H.P. et al., 2002a. Phosphorus sources, speciation and dynamics in the lowland eutrophic River Kennet, UK. Science of the Total Environment, 282: 175-203.

Jarvie, H.P., Withers, P.J.A., Neal, C., 2002b. Review of robust measurement of phosphorus in river water: sampling, storage, fractionation and sensitivity. Hydrology and Earth System Sciences, 6(1): 113-131.

Johnes, D., 2011. FATHOM - Matlab toolbox for Multivariate Ecological & Oceanographic Data Analysis.

Johnes, P., 2007. Uncertainties in annual riverine phosphorus load estimation: Impact of load estimation methodology, sampling frequency, baseflow index and catchment population density. Journal of Hydrology: 241-258.

Jordan, P., Arnscheidt, A., McGrogan, H., McCormick, S., 2007. Characterising phosphorus transfers in rural catchments using a continuous bank-side analyser. Hydrology and Earth System Sciences, 11(1): 372-381.

Jordan, P., Arnscheidt, J., McGrogan, H., McCormick, S., 2005. High-resolution phosphorus transfers at the catchment scale: the hidden importance of non-storm transfers. Hydrology and Earth System Sciences, 9(6): 685-691.

Jordan, P., Cassidy, R., 2011. Technical Note: Assessing a 24/7 solution for monitoring water quality loads in small river catchments. Hydrology and Earth System Sciences, 15(10): 3093-3100.

Kaser, D., Binley, A., Heathwaite, A., Krause, S., 2009. Spatio-temporal variations of hyporheic flow in a riffle-step-pool sequence. Hydrological Processes: 2138-2149.

Kirchner, J., Feng, X., Neal, C., Robson, A., 2004. The fine structure of water-quality dynamics: the (high-frequency) wave of the future. Hydrological Processes: 1353-1359.

Kirchner, J.W., Neal, C., 2013. Universal fractal scaling in stream chemistry and its implications for solute transport and water quality trend detection. Proceedings of the National Academy of Sciences, 110(30): 12213-12218.

Krause, S., Tecklenburg, C., Munz, M., Naden, E., 2013. Streambed nitrogen cycling beyond the hyporheic zone: Flow controls on horizontal patterns and depth distribution of nitrate and dissolved oxygen in the upwelling groundwater of a lowland river. Journal of Geophysical Research-Biogeosciences, 118(1): 54-67.

Lawler, D.M., Petts, G.E., Foster, I.D.L., Harper, S., 2006. Turbidity dynamics during spring storm events in an urban headwater river system: The Upper Tame, West Midlands, UK. Science of the Total Environment, 360(1-3): 109-126.

LCM2007, 2011. Land cover map 2007. Raster data - Great Britain.

Legendre, L., Legendre, P., 1998. Numerical ecology. Elsevier Scientific Pub. Co., Amsterdam, 853 pp.

Legendre, P., Anderson, M.J., 1999. Distance-Based Redundancy Analysis: Testing Multispecies Responses in Multifactorial Ecological Experiments. 69(1): 1-24.

Manly, B.F.J., 2007. Randomization, Bootstrap and Monte Carlo Methods in Biology, 3rd Edition. CRC PressINC.

McDaniel, M.D., David, M.B., Royer, T.V., 2009. Relationships between Benthic Sediments and Water Column Phosphorus in Illinois Streams. Journal of Environmental Quality, 38(2): 607-617.

McDiffett, W.F., Beidler, A.W., Dominick, T.F., McCrea, K.D., 1989. Nutrient concentration-stream discharge relationships during storm events in a 1st-order stream. Hydrobiologia, 179(2): 97-102.

Mellander, P.-E. et al., 2012. Quantifying nutrient transfer pathways in agricultural catchments using high temporal resolution data. Environmental Science & Policy, 24: 44-57.

Minella, J.P.G., Merten, G.H., Reichert, J.M., Clarke, R.T., 2008. Estimating suspended sediment concentrations from turbidity measurements and the calibration problem. Hydrological Processes, 22(12): 1819-1830.

Mulholland, P.J., 1992. Regulation of nutrient concentrations in a tempterate forest stream - roles of upland, riparian, and instream processes. Limnology and Oceanography, 37(7): 1512-1526.

Murphy, J., Riley, J.P., 1962. A modified single solution method for determination of phosphate in natural waters. Analytica Chimica Acta, 27(1): 31-36.

Naden, P.S., 2010. The Fine-Sediment Cascade, Sediment Cascades. John Wiley & Sons, Ltd, pp. 271-305.
Neal, C. et al., 2010a. Declines in phosphorus concentration in the upper River Thames (UK): Links to sewage effluent cleanup and extended end-member mixing analysis. Science of the Total Environment: 1315-1330.
Neal, C., Jarvie, H.P., Withers, P.J.A., Whitton, B.A., Neal, M., 2010b. The strategic significance of wastewater sources to pollutant phosphorus levels in English rivers and to environmental management for rural, agricultural and urban catchments. Science of the Total Environment, 408(7): 1485-1500.
Neal, C. et al., 2012. High-frequency water quality time series in precipitation and streamflow: From fragmentary signals to scientific challenge. Science of the Total Environment, 434: 3-12.
Oeurng, C., Sauvage, S., Sánchez-Pérez, J.-M., 2010. Temporal variability of nitrate transport through hydrological response during flood events within a large agricultural catchment in south-west France. Science of The Total Environment, 409(1): 140-149.
Palmer-Felgate, E.J. et al., 2008. Phosphorus dynamics and productivity in a sewage-impacted lowland chalk stream. Journal of Hydrology, 351(1-2): 87-97.
Palmer-Felgate, E.J., Jarvie, H.P., Withers, P.J.A., Mortimer, R.J.G., Krom, M.D., 2009. Stream-bed phosphorus in paired catchments with different agricultural land use intensity. Agriculture, Ecosystems & Environment, 134(1–2): 53-66.
Partech, 2013. WaterWatch multiparameter meter http://www.partech.co.uk/products/7300w2.html, UK.
Petticrew, E.L., Krein, A., Walling, D.E., 2007. Evaluating fine sediment mobilization and storage in a gravel-bed river using controlled reservoir releases. Hydrological Processes, 21(2): 198-210.
Rothwell, J.J. et al., 2010. A spatial and seasonal assessment of river water chemistry across North West England. Science of the Total Environment, 408(4): 841-855.
Rozemeijer, J.C. et al., 2010. Improving Load Estimates for NO3 and P in Surface Waters by Characterizing the Concentration Response to Rainfall Events. Environmental Science & Technology, 44(16): 6305-6312.
Scott, C. et al., 2001. Residual phosphorus in runoff from successional forest on abandoned agricultural land: 1. Biogeochemical and hydrological processes. Biogeochemistry, 55(3): 293-310.
Siwek, J., Siwek, J.P., Żelazny, M., 2012. Environmental and land use factors affecting phosphate hysteresis patterns of stream water during flood events (Carpathian Foothills, Poland). Hydrological Processes.
Stutter, M.I., Lumsdon, D.G., 2008. Interactions of land use and dynamic river conditions on sorption equilibria between benthic sediments and river soluble reactive phosphorus concentrations. Water Research, 42(16): 4249-4260.
Systea, 2013. MicroMac C Analyser, Multiparameter colorimetric analyser - http://www.partech.co.uk/products/micromac_c.html.
Thompson, J.J.D., Doody, D.G., Flynn, R., Watson, C.J., 2012. Dynamics of critical source areas: does connectivity explain chemistry? The Science of the total environment, 435-436: 499-508.
Thompson, S.E., Basu, N.B., Lascurain, J., Jr., Aubeneau, A., Rao, P.S.C., 2011. Relative dominance of hydrologic versus biogeochemical factors on solute export across impact gradients. Water Resources Research, 47.
Vitousek, P.M. et al., 1997. Human alteration of the global nitrogen cycle: Sources and consequences. Ecological Applications, 7(3): 737-750.

Wade, A.J. et al., 2012a. From existing in situ, high-resolution measurement technologies to lab-on-a-chip – the future of water quality monitoring? Hydrol. Earth Syst. Sci. Discuss., 9(5): 6457-6506.

Wade, A.J. et al., 2012b. Hydrochemical processes in lowland rivers: insights from in situ, high-resolution monitoring. Hydrology and Earth System Sciences, 16(11): 4323-4342.

Walling, D.E., Webb, B.W., 1982. Sediment availability and the prediction of storm-period sediment yields. Hydrological Sciences Journal-Journal Des Sciences Hydrologiques, 27(2): 246-246.

Whitehead, P.G., Crossman, J., 2012. Macronutrient cycles and climate change: Key science areas and an international perspective. Science of the Total Environment, 434: 13-17.

Table 1 Descriptors of hysteresis loops and hydrological, biogeochemical and antecedent conditions characteristics of the storm events (characteristics derivation in Supporting Table A) and Pearson's correlations with hysteresis direction and magnitude (Supporting Table G). Significant correlations in bold (at α = 0.05 level)

	Parameters	Description	Units	Hysteresis direction			Hysteresis magnitude		
				TP	**TRP**	**TP**	**TRP**	**TP**	**TRP**
Hysteresis descriptors	ΔR	rotational parameter[a]	%						
	pHW	response factor[b]	mmol $m^{-6}s2$						
	pB	response factor[b]	mmol $m^{-6}s2$						
	ΔC	magnitude parameter[c]	%						
	h	magnitude factor[d]	mmol m^{-3}						
	g	gradient factor[d]	mmol s^{-1}						
Hydrological properties	H_{mean}	mean stage	m	**0.54**	**0.47**	**0.52**	0.12	-0.01	-0.06
	Q_{max}	maximum discharge during the storm event	m^3s^{-1}	**0.37**	**0.25**	**0.39**	0.06	0.19	0.15
	Q_{vol}	volume of discharge during the storm event	10^3m^3	**0.64**	**0.45**	**0.60**	-0.09	0.16	0.10
	Q_{mean}	average discharge during the storm event	m^3s^{-1}	**0.35**	**0.38**	**0.33**	**-0.32**	-0.20	-0.16
	ΔQ_t	magnitude of the storm event	%	**0.39**	0.18	**0.38**	0.04	**0.34**	-0.03
	ΔQ_{t-1}	magnitude of the preceding storm event	%	**0.31**	**0.29**	**0.27**	-0.12	-0.04	0.00
	RL	relative duration of the rising limb	%	0.11	0.05	**0.21**	**-0.32**	-0.04	-0.18
	k	slope of the initial phase of the recession limb	m^3s^{-1}	**0.37**	**0.23**	**0.38**	0.07	0.20	0.15

	t	duration of the storm event	h	**0.29**	**0.26**	**0.27**	-0.09	**-0.36**	-0.20
	Δt	time from the previous storm event	days	-0.08	-0.18	-0.07	**0.33**	**0.37**	0.16
	Load	nutrient load	10^2kg	**0.50**	**0.27**	**0.52**	**-0.24**	**-0.30**	0.21
Biogeochemical properties	m	mean slope of rising and falling *c*-*q* limbs in log-space	-	**-0.29**	**-0.54**	0.00	**-0.53**	**-0.65**	**-0.54**
	C_0	baseline nutrient concentration prior to the storm event	μgl^{-1} or NTU	0.09	**-0.21**	0.19	**0.57**	**0.31**	0.02
	C_{max}	maximum nutrient concentration during the storm event	μgl^{-1} or NTU	0.16	-0.11	0.10	**0.81**	**0.67**	**0.37**
	C_{mean}	mean nutrient concentration during the storm event	μgl^{-1} or NTU	0.16	**-0.21**	0.20	**0.53**	**0.32**	0.02
	$COND_{mean}$	mean specific conductivity during the storm event	μScm^{-1}	-0.11	-0.19	-0.02	0.06	0.11	0.28
	pH_{mean}	mean pH during the storm event	-	**0.56**	**0.52**	**0.59**	-0.11	-0.09	0.09
	DO_{mean}	mean dissolved oxygen concentration during the storm event	%	**0.62**	**0.55**	**0.57**	-0.10	-0.18	0.05
	RED_{mean}	mean redox potential during the storm event	mV	**-0.24**	**-0.28**	**-0.28**	0.10	0.16	0.06
Antecedent conditions	$TEMPW_{mean}$	mean stream water temperature during the storm event	°C	**-0.54**	**-0.57**	**-0.54**	**0.34**	**0.39**	-0.02
	$TEMPA_{mean}$	mean air temperature during the storm event	°C	**-0.54**	**-0.58**	**-0.55**	**0.35**	**0.39**	-0.02
	RAD_{mean}	mean solar radiation during the storm event	Wm^{-2}	**-0.50**	**-0.53**	**-0.52**	**0.42**	**0.33**	0.11
	$RAIN_{tot}$	total amount of rainfall for the event	mm	-0.11	-0.15	-0.12	**0.39**	**0.61**	0.10
	$RAIN_{int\_mean}$	average rainfall intensity	mm h^{-1}	-0.09	-0.12	-0.05	**0.38**	**0.29**	0.12
	$RAIN_{int\_max}$	maximum rainfall intensity	mm h^{-1}	**-0.25**	**-0.34**	-0.20	**0.33**	**0.36**	0.15
	$\Delta RAIN$	rainfall duration	h	0.03	-0.01	0.09	0.12	**0.41**	-0.09
	Q_0	baseline discharge prior to the storm event	m^3s^{-1}	0.19	**0.23**	0.15	**-0.24**	**-0.40**	-0.12

API_7	seven day antecedent precipitation	mm	**-0.24**	-0.10	**-0.22**	**-0.27**	**-0.36**	**-0.38**

[a] *ΔR* is the product of the direction of the hysteresis and the normalised area of the hysteresis loop, calculated as the polygon area of the convex hull of standardised c-q points (Butturini *et al.*, 2006)

[b] *pHW* (House and Warwick, 1998) and *pB* (Bowes *et al.*, 2005) are empirical parameters that indicate the direction of hysteresis loops: clockwise for positive values and anti-clockwise for negative values. The absolute value of the response parameter controls the range of concentration values and thus indicates the shape and size of the hysteresis loop

[c] *ΔC* is the relative percentage concentration change between C_{max} and C_0 during the storm event (Butturini *et al.*, 2006)

[d] *h* (House and Warwick, 1998) and *g* (Bowes *et al.*, 2005) are empirical parameters that indicate the magnitude of a hysteresis loop in terms of the size of the loop along the concentration axis

Table 2 Spearman rho correlation coefficients between hysteresis descriptors (ΔR, p_{HW}, ΔC and h) and hydrological, biogeochemical and antecedent meteorological characteristics. Significant p values in bold (at α = 0.05 level)

		Hysteresis direction						Hysteresis magnitude					
		ΔR			p_{HW}			ΔC			h		
		TP	**TRP**	**TURB**	**TP**	**TRP**	**TURB**	**TP**	**TRP**	**TURB**	**TP**	**TRP**	**TURB**
Hysteresis descriptors	***pHW***	**0.69**	**0.61**	**0.59**									
	ΔC	**0.24**	0.14	**0.49**	0.05	0.02	**0.29**						
	h	0.04	-0.17	**0.32**	-0.09	**-0.27**	0.03	**0.48**	**0.33**	**0.58**			
Hydrological properties	Q_{max}	**0.57**	**0.56**	**0.56**	**0.44**	**0.43**	0.20	-0.02	0.02	**0.52**	-0.13	**-0.26**	**0.61**
	Q_{vol}	**0.68**	**0.62**	**0.62**	**0.49**	**0.48**	**0.28**	0.04	0.11	**0.59**	-0.09	**-0.24**	**0.55**
	Q_{mean}	**0.55**	**0.55**	**0.53**	**0.45**	**0.44**	0.16	-0.07	-0.06	**0.44**	-0.12	**-0.26**	**0.59**
	Q_t	**0.43**	**0.27**	**0.44**	0.19	0.14	**0.25**	**0.40**	**0.53**	**0.60**	0.02	-0.08	**0.31**
	Q_{t-1}	0.21	**0.26**	0.14	0.11	0.07	0.21	0.18	0.05	0.08	-0.17	-0.14	-0.12
	RL	0.13	0.16	0.19	0.14	0.07	-0.05	-0.18	-0.04	-0.06	-0.12	-0.11	0.03
	k	**0.55**	**0.54**	**0.60**	**0.45**	**0.43**	0.20	-0.04	0.02	**0.50**	-0.16	**-0.25**	**0.59**
	t	0.21	0.08	0.16	0.07	0.04	**0.33**	**0.27**	**0.45**	**0.37**	0.03	0.02	-0.13
	Δt	-0.21	-0.22	-0.18	-0.08	-0.07	0.03	0.22	**0.31**	-0.11	-0.02	0.02	**-0.44**
	Load	**0.70**	**0.59**	**0.61**	**0.52**	**0.44**	**0.32**	0.18	0.20	**0.66**	0.11	0.00	**0.65**
chemic al proper	m	-0.14	**-0.33**	-0.01	-0.08	**-0.27**	0.14	**0.42**	0.22	0.21	**0.50**	**0.43**	**0.24**
	C_{max}	**0.28**	0.07	**0.42**	0.09	-0.04	**0.25**	**0.79**	**0.67**	**0.87**	**0.74**	**0.82**	**0.76**

	C_{mean}	**0.26**	-0.01	**0.30**	0.12	-0.12	0.17	**0.45**	**0.31**	**0.59**	**0.75**	**0.83**	**0.78**
	$COND_{mean}$	**-0.44**	**-0.41**	**-0.40**	**-0.25**	**-0.26**	-0.08	-0.09	-0.03	**-0.34**	-0.08	0.15	**-0.49**
	pH_{mean}	**0.36**	**0.36**	**0.28**	**0.28**	**0.30**	**0.23**	0.07	0.00	**0.30**	**-0.28**	**-0.32**	0.14
	DO_{mean}	0.22	0.20	0.16	**0.24**	**0.33**	**0.31**	0.10	0.00	0.20	-0.03	-0.18	-0.13
	RED_{mean}	-0.18	-0.19	-0.20	**-0.38**	**-0.32**	**-0.23**	0.06	0.08	-0.19	-0.05	0.10	-0.21
	$TEMPW_{mean}$	**-0.57**	**-0.49**	**-0.54**	**-0.63**	**-0.64**	**-0.31**	0.12	0.20	**-0.36**	0.21	**0.42**	**-0.25**
Antecedent conditions	$TEMPA_{mean}$	**-0.56**	**-0.50**	**-0.55**	**-0.62**	**-0.64**	**-0.31**	0.11	0.19	**-0.36**	**0.26**	**0.47**	**-0.26**
	RAD_{mean}	**-0.51**	**-0.42**	**-0.48**	**-0.53**	**-0.56**	**-0.24**	0.12	0.19	**-0.29**	**0.23**	**0.41**	-0.15
	$RAIN_{tot}$	-0.12	-0.15	0.01	-0.18	-0.17	0.10	**0.32**	**0.47**	0.06	0.14	**0.31**	0.01
	$RAIN_{int\_mean}$	-0.09	-0.10	-0.04	**-0.28**	**-0.27**	-0.04	**0.46**	**0.32**	0.16	**0.39**	**0.39**	**0.26**
	$RAIN_{int\_max}$	-0.21	-0.20	-0.06	**-0.33**	**-0.34**	-0.03	**0.31**	**0.30**	0.00	0.17	**0.36**	0.08
	$\Delta RAIN$	0.09	0.02	0.20	0.02	-0.01	0.22	0.05	0.22	0.04	0.04	0.24	0.02
	Q_0	**0.45**	**0.47**	**0.40**	**0.39**	**0.41**	0.08	-0.16	-0.23	0.24	-0.08	-0.22	**0.51**
	API_7	-0.10	0.05	-0.05	-0.01	0.06	-0.07	**-0.29**	**-0.26**	**-0.28**	-0.08	0.10	0.04

Table 3 If-then statements for the fuzzy logic inference system. Direction of the hysteresis loops: A – anti-clockwise, C – clockwise

Membership rule	**Mean discharge volume is**	**Operator**	**Mean air temperature is**	**Then, the direction of the hysteresis is**
1	low	and	high	A
2	low	and	medium	A
3	low	and	low	A
4	medium	and	high	A
5	medium	and	medium	C
6	medium	and	low	C
7	high	and	high	C
8	high	and	medium	C
9	high	and	low	C

Table 4 Comparison between the nutrients' hysteresis direction (A - anti-clockwise, Nh – no hysteresis, C - clockwise) established by visual inspection, fuzzy logic inference system (FIS) and optimisation parameters. Percentage of A and C storm events per season based on the FIS results: Win - winter A 25% and C 75% (December-February), Spr – spring A 63% and C 38% (March-May), Sum – summer A 89% and C 11% (June-August), Aut – autumn A 52% and C 48% (September-November). For the FIS both the degree of membership and direction of hysteresis (*D*) were given. Inconsistent hysteresis patterns between (observed vs. predicted by the FIS) highlighted in grey

	Season	**Visual inspection**			**Fuzzy inference**		**Optimisation**					
							p_{HW}			p_B		
		TP	**TRP**	**TURB**	**Memb.**	***D***	**TP**	**TR**	**TURB**	**TP**	**TRP**	**TURB**
1	Sum	A	A	A	-0.99	A	A	A	C	A	A	C
2	Sum	A	A	A	-1.00	A	A	A	A	A	A	A
3	Sum	-	A	A	-0.94	A	-	A	A	-	A	A
4	Sum	C	C	C	1.00	C	C	C	C	C	C	C
5	Sum	A	A	A	-0.96	A	A	A	A	A	A	A
6	Sum	-	A	A	-0.99	A	-	A	A	-	A	C
7	Sum	-	Nh	Nh	-0.36	A	-	C	C	-	C	C
8	Sum	-	A	A	-0.91	A	-	C	C	-	A	A
9	Sum	-	Nh	C	0.95	C	-	A	C	-	C	C
10	Aut	C	C	C	0.84	C	C	C	C	C	C	C
11	Aut	Nh	Nh	Nh	-0.84	A	A	A	A	C	C	A
12	Aut	C	C	C	0.94	C	C	C	C	C	C	C
13	Aut	Nh	Nh	Nh	1.00	C	A	A	A	C	C	C
14	Aut	Nh	Nh	Nh	-0.58	A	A	C	A	C	C	A
15	Aut	A	-	Nh	-0.92	A	A	-	A	A	-	A
16	Aut	C	-	C	0.97	C	C	-	C	A	-	C
17	Aut	A	-	A	-0.87	A	C	-	C	C	-	C
18	Win	C	C	C	0.99	C	C	C	C	C	C	C
19	Win	C	C	C	0.86	C	C	C	C	C	C	C
20	Win	A	A	A	-0.98	A	A	A	A	C	C	C
21	Win	-	C	C	0.92	C	-	C	C	-	C	C
22	Win	A	A	C	-0.92	A	C	A	C	C	C	C
23	Spr	Nh	C	A	-0.20	A	A	C	A	C	C	A
24	Spr	A	A	A	-0.64	A	A	C	A	A	C	A
25	Sum	A	A	A	-0.99	A	A	A	A	A	A	A
26	Sum	A	A	A	-0.95	A	A	A	A	A	A	A
27	Sum	A	A	A	-0.97	A	A	A	C	A	A	C

28	Sum	A	A	A	-1.00	A	A	A	A	A	A	A
29	Sum	A	A	A	-0.95	A	A	A	C	A	A	A
30	Aut	A	A	-	-0.99	A	A	A	-	A	A	-
31	Aut	A	A	-	-0.97	A	A	A	-	A	A	-
32	Aut	C	C	C	-0.86	A	C	C	C	C	C	C
33	Aut	C	C	C	-0.94	A	C	C	C	C	C	C
34	Aut	C	C	Nh	-0.85	A	C	C	C	C	C	C
35	Aut	Nh	Nh	Nh	-0.71	A	A	A	C	A	A	C
36	Aut	C	Nh	C	0.99	C	C	C	C	C	C	C
37	Aut	Nh	C/Nh	C	-0.85	A	C	C	C	C	C	C
38	Aut	A	A	A	-0.98	A	A	A	C	C	C	C
39	Aut	C	C	C	0.32	C	C	C	C	C	C	C
40	Aut	C	C	C	0.90	C	C	C	C	C	C	C
41	Aut	C	C	C/Nh	0.94	C	C	C	C	C	C	C
42	Aut	-	A/Nh	C/Nh	0.88	C	-	A	C	-	C	C
43	Aut	Nh	Nh	Nh	0.00	C	A	A	A	C	C	C
44	Aut	Nh	A/Nh	Nh	0.90	C	C	C	A	C	A	C
45	Win	A	A	A	-0.09	A	C	C	C	C	C	C
46	Win	C/Nh	C	C	0.98	C	C	C	C	C	C	C
47	Win	C	C	C	1.00	C	C	C	C	C	C	C
48	Win	C	A	C	0.99	C	C	A	C	A	A	A
49	Win	C	C	C	0.96	C	C	A	C	C	C	C
50	Win	Nh	Nh	Nh	0.87	C	C	C	C	C	C	C
51	Win	C	C	C	0.37	C	C	C	C	C	C	C
52	Spr	C	C	C	0.19	C	C	C	C	C	C	C
53	Spr	C	C	C	0.92	C	C	C	C	C	C	C
54	Spr	Nh	A	Nh	-0.97	A	A	A	C	A	A	C
55	Spr	Nh	Nh	Nh	-0.86	A	A	A	C	A	A	C
56	Spr	C	C	C	0.95	C	C	C	C	C	C	C
57	Spr	C	C	C	-0.57	A	C	C	C	C	C	C
58	Sum	A	A	A	-0.95	A	A	A	A	A	A	A
59	Sum	A	A	A	-1.00	A	A	A	A	A	A	A
60	Sum	A	A	A	-1.00	A	A	A	A	A	A	A
61	Sum	A	Nh	Nh	-0.98	A	A	A	A	A	A	C

Figure 1 Examples of TP *c-q* hysteresis loops: chemograph (TP time series, black line) and hydrograph (Q time series, blue line) for the storm event 16 with indication of the rising limb (RL), falling limb (FL) and the time lag (TL) (a), clockwise storm event 16 (b), anti-clockwise storm event 31 (c), no hysteresis storm event 13 (d) and anti-clockwise “figure 8” storm event 38 (e). Number labels indicate elapsed time from the beginning of the storm event in hours and circular arrows show the direction of clockwise and anti-clockwise hysteresis loops

Figure 2 Time series of flow discharge (top), TP concentration (middle) and Q-TP scatter plots with selected hysteresis loops highlighted. All data shown on logarithmic scale. The storms are numbered as in Supporting Table B. Observed gaps in TP concentration time series indicate periods when the in situ lab was not operational due to freezing or instruments malfunction

Figure 3 Box plots of slope (a), discharge volume (b), maximum concentration (c), hysteresis magnitude ΔC(d air temperature (e) and specific conductivity (f) for anti-clockwise (A), no hysteresis (Nh) and clockwise (C) hysteresis patterns. The central red thick line – mean, the edges of the box indicate 25 and 75 percentiles, whiskers extend to the most extreme data points. Please note that for plots a-c the vertical axes are broken to show the most extreme values. At the top of each subplot are *p* values for Kruskal-Wallis analysis of variance between storm event groups (A, Nh, C) based on Supporting Table D

Figure 4 TP redundancy analysis distance biplot showing ordination of selected explanatory and response variables. The length of explanatory vectors indicates strength of the relationship with the site scores of canonical axes. Distances among storm events are approximations of their Euclidean distances. Projecting a storm event at the right angle onto the response vector approximates a value of the storm event along that vector. The angles between response and explanatory vectors indicate their correlation (Legendre and Legendre, 1998)

Figure 5 Membership functions for discharge volume (top), mean air temperature (middle) and hysteresis direction (bottom)

Figure 6 Box plots of hysteresis direction (ΔR) for TP, TRP and TURB (a), air temperature (b) and discharge volume (c) for each season. The central red thick line – mean, the edges of the box indicate 25 and 75 percentiles, whiskers extend to the most extreme data points. At the top of each subplot are *p* values for Kruskal-Wallis analysis of variance between seasons (3 d.f.)

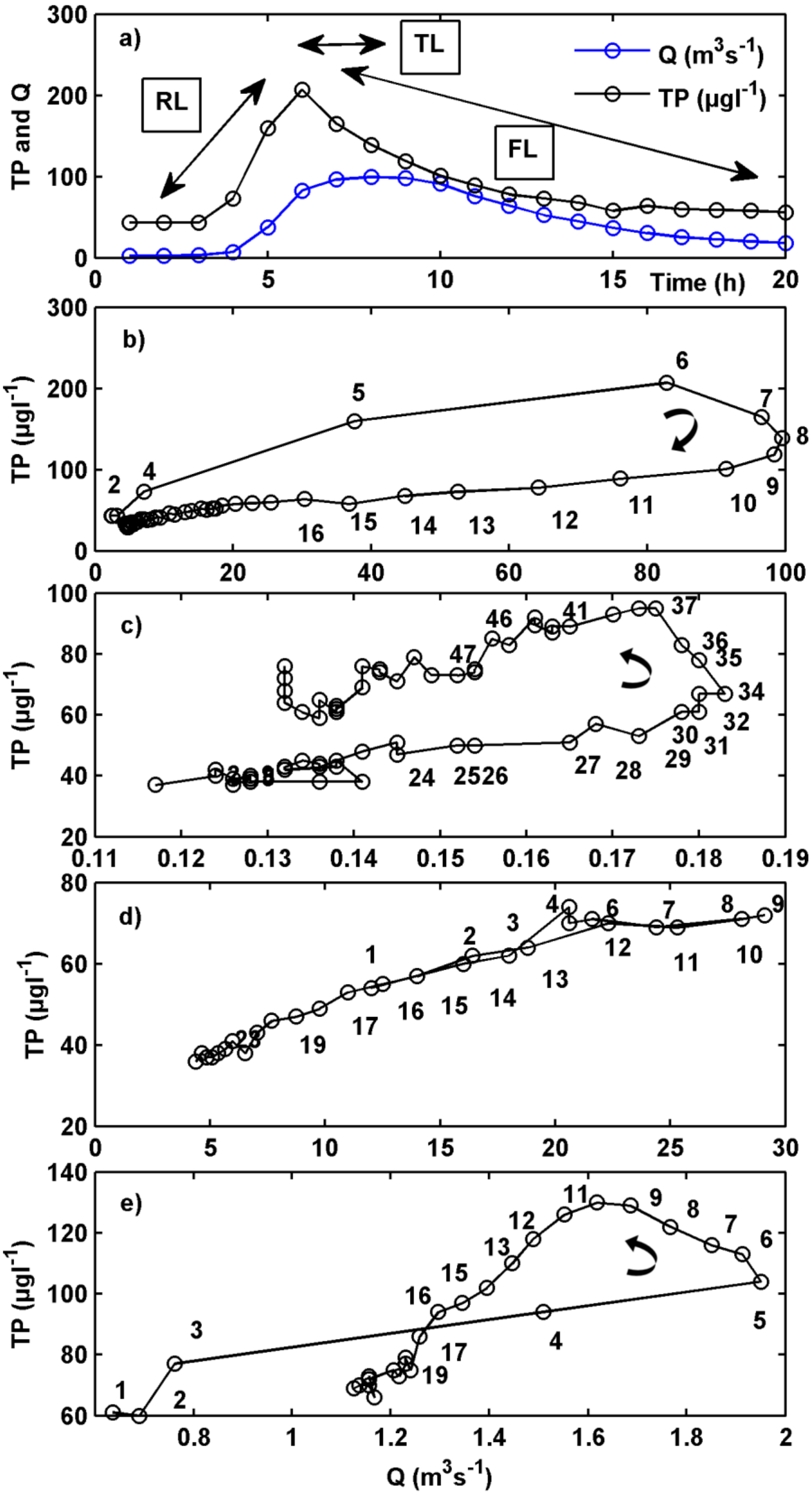
a)
RL
TL
FL
Q (m3s-1)
TP (µgl-1)
TP and Q
Time (h)
b)
TP (µgl-1)
c)
TP (µgl-1)
d)
TP (µgl-1)
e)
TP (µgl-1)
Q (m3s-1)

Figure 1

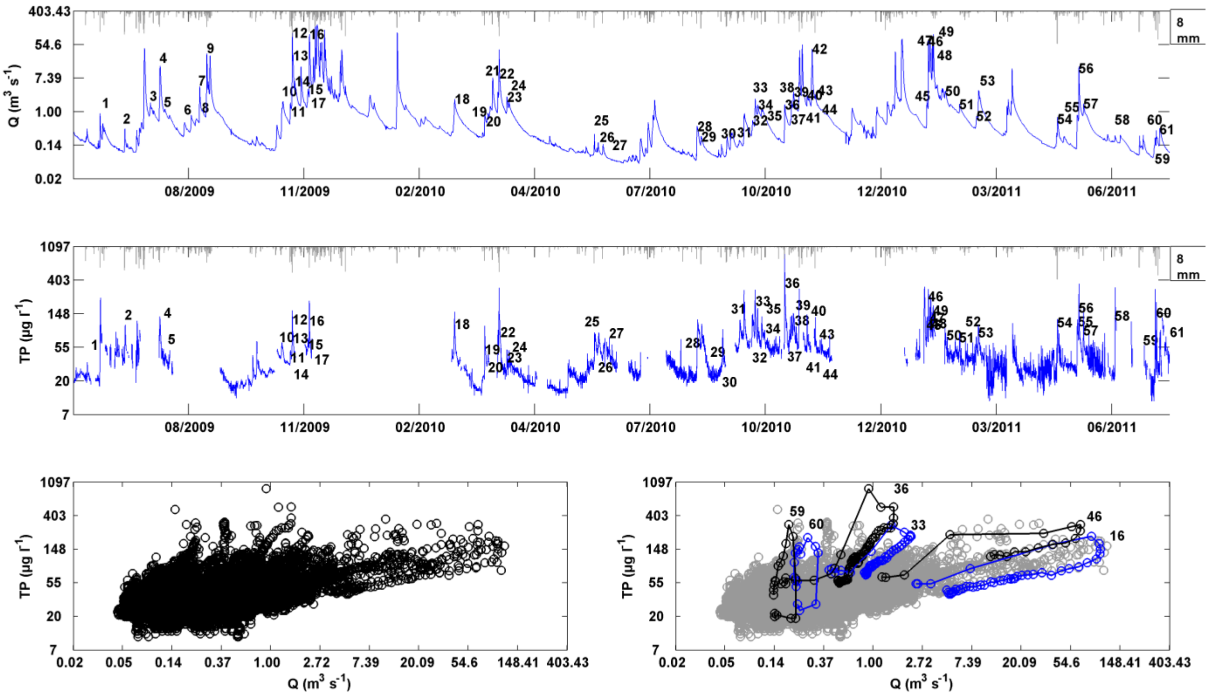
Q (m^3 s^{-1})
TP (µg l^{-1})
8 mm
08/2009
11/2009
02/2010
04/2010
07/2010
10/2010
12/2010
03/2011
06/2011
Q (m^3 s^{-1})

Figure 2

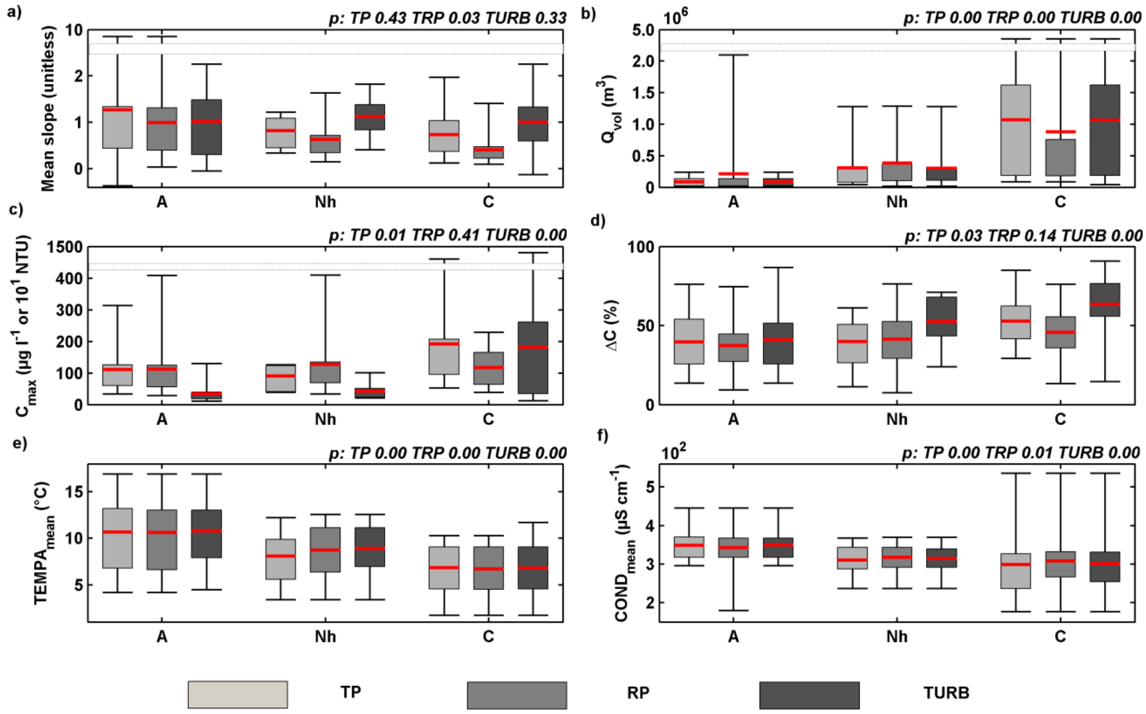

a)
p: TP 0.43 TRP 0.03 TURB 0.33
Mean slope (unitless)
b)
p: TP 0.00 TRP 0.00 TURB 0.00
Q vol (m3)
c)
p: TP 0.01 TRP 0.41 TURB 0.00
C max (µg l-1 or 10-1 NTU)
d)
p: TP 0.03 TRP 0.14 TURB 0.00
ΔC (%)
e)
p: TP 0.00 TRP 0.00 TURB 0.00
TEMPA mean (°C)
f)
p: TP 0.00 TRP 0.01 TURB 0.00
COND mean (µS cm-1)
A
Nh
C
TP
RP
TURB

Figure 3

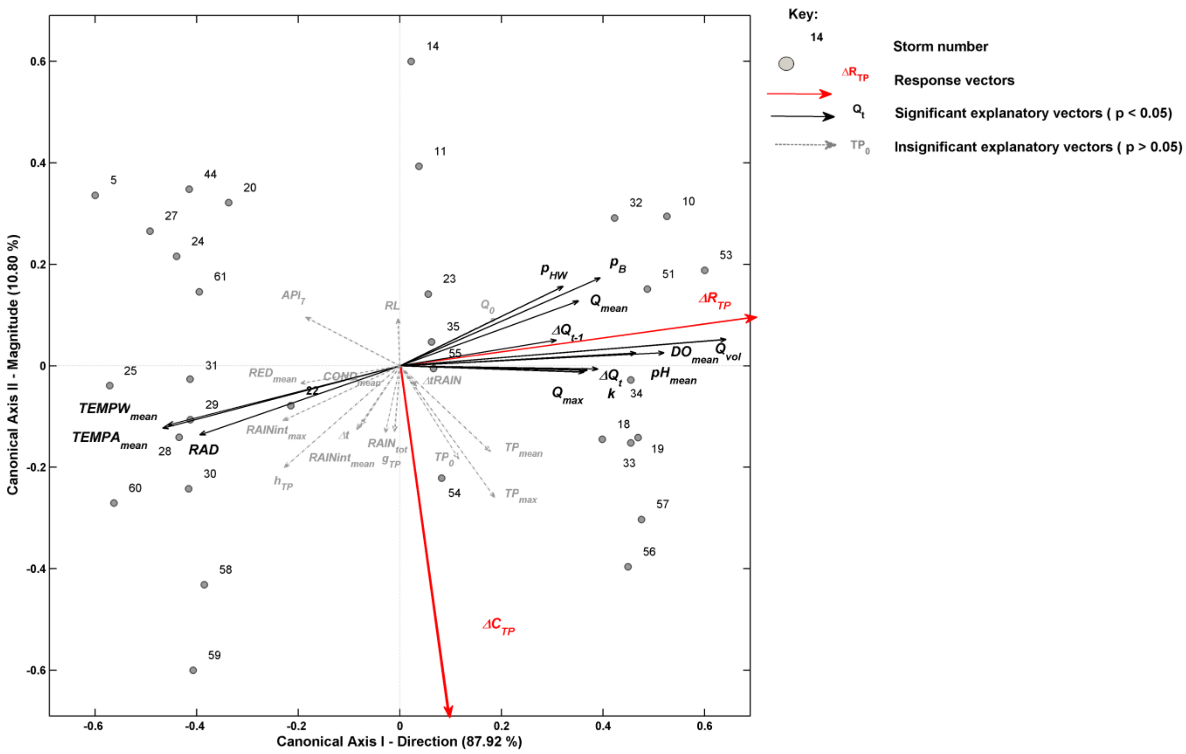

Key:
14
Storm number
ΔR_TP
Response vectors
Q_t
Significant explanatory vectors (p < 0.05)
TP_0
Insignificant explanatory vectors (p > 0.05)
Canonical Axis I - Direction (87.92 %)
Canonical Axis II - Magnitude (10.80 %)
ΔR_TP
ΔC_TP
p_HW
p_B
Q_mean
ΔQ_t-1
DO_mean
Q_vol
pH_mean
ΔQ_t
k
Q_max
TEMPW_mean
TEMPA_mean
RAD
API_7
RL
Q_0
RED_mean
COND_mean
ΔtRAIN
RAINint_max
Δt
RAIN_tot
RAINint_mean
g_TP
TP_0
TP_mean
TP_max
h_TP

Figure 4

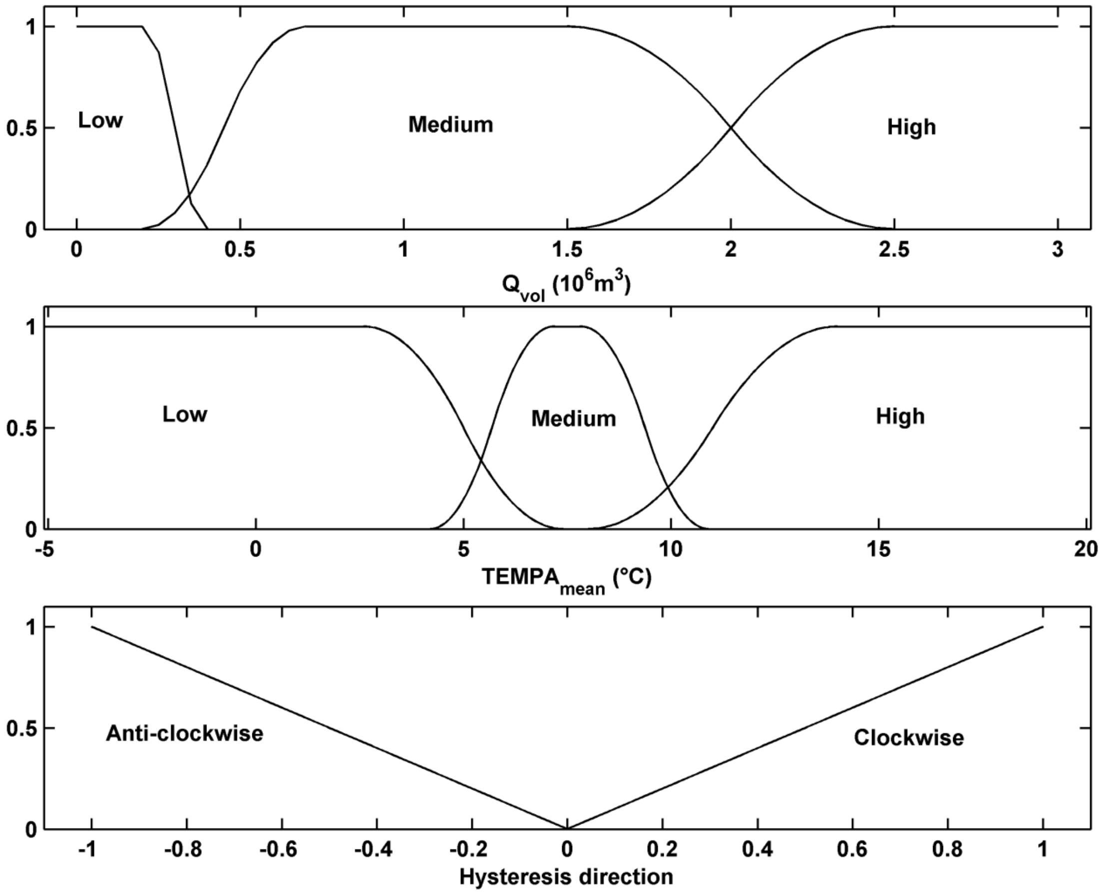

1
0.5
0
Low
Medium
High
0
0.5
1
1.5
2
2.5
3
Q_vol (10^6 m^3)
1
0.5
0
Low
Medium
High
-5
0
5
10
15
20
TEMPA_mean (°C)
1
0.5
0
Anti-clockwise
Clockwise
-1
-0.8
-0.6
-0.4
-0.2
0
0.2
0.4
0.6
0.8
1
Hysteresis direction

Figure 5

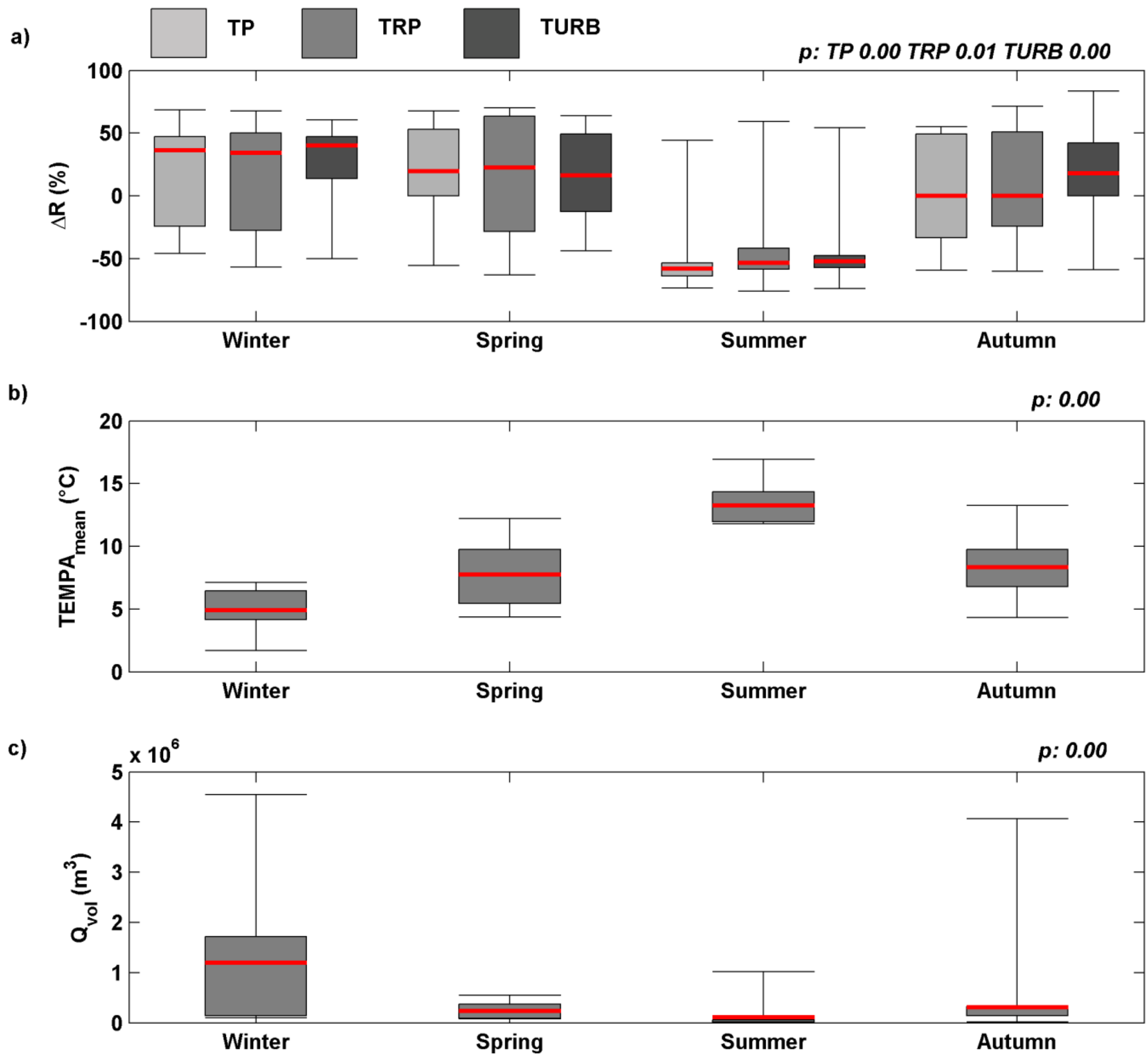

a)
TP
TRP
TURB
p: TP 0.00 TRP 0.01 TURB 0.00
ΔR (%)
100
50
0
-50
-100
Winter
Spring
Summer
Autumn
b)
p: 0.00
TEMPA mean (°C)
20
15
10
5
0
Winter
Spring
Summer
Autumn
c)
x 10^6
p: 0.00
Q vol (m^3)
5
4
3
2
1
0
Winter
Spring
Summer
Autumn

Figure 6

Supporting Table A Descriptors of the hysteresis loops and hydrological and biogeochemical characteristics of the storm events

Parameters	Abbreviation	Definition	Eq.
Hysteresis direction	***ΔR***	rotational parameter which is the product of the direction of the hysteresis *R* (-1 anti-clockwise, 0 no hysteresis or unclear pattern, 1 clockwise) and the normalised area of the hysteresis loop A_h, calculated as the polygon area of the convex hull of standardised c-q points (Butturini et al., 2006) $$\Delta R = R * A_h * 100$$	(1)
	pHW ***pB***	response factors *pHW* (House and Warwick, 1998) and *pB* (Bowes et al., 2005). Positive values indicate a clockwise hysteresis, whereas negative values indicate anti-clockwise hysteresis. The absolute value of the response parameter controls the range of concentration values (maximum and minimum) and thus indicates the shape and size of the hysteresis loop, i.e. *pHW* or *pB* values close to zero are pertinent to small hysteretic loops with a near linear c-q response The parameters are calculated by optimising the following formulas: $$C(t) = C_d(t) + p_{HW}\frac{dQ(t)}{dt}\frac{(Q(t) - Q_0)}{Q(t)} + h\frac{(Q(t) - Q_0)}{Q(t)}$$ $$C(t) = C_d(t) + p_B\frac{dQ(t)}{dt} + g\frac{(Q(t) - Q_0)}{Q_0 Q(t)}$$ Where *C(t)* is the nutrient concentration, $C_d(t)$ expresses the dilution effect which is a ratio of baseline instantaneous nutrient load (Q_0*C_0) to discharge at time *t* (*Q(t)*), *dQ(t)/dt* is a rate of change of discharge during the storm event, the values of C_0 and Q_0 were assigned as the initial nutrient concentration and stream discharge respectively in the beginning of the hydrograph.	(2) (3)
Hysteresis magnitude	***ΔC***	magnitude parameter which is the relative percentage concentration change between C_{max} and C_0 during the storm event (Butturini et al., 2006) $$\Delta C = \frac{C_{max} - C_0}{C_{max}} * 100$$	(4)
	h ***g***	magnitude *h* (House and Warwick, 1998) and gradient *g* (Bowes et al., 2005) factors. They control the maximum concentration level, “stretching” (for higher values of *h* and *g*) or “shrinking” (for lower values of *h* and *g*) of the hysteresis loop along the concentration axis. Calculated as per equations 1 and 2	
Hydrological properties	Q_0	baseline discharge prior to the storm event	
	Q_{max}	maximum discharge during the storm event	
	Q_{vol}	volume of discharge during the storm event	
	Q_{mean}	average discharge during the storm event	
	ΔQ_t	magnitude of the storm event calculated as a relative percentage difference between Q_0 and Q_{max} $$\Delta Q_t = \frac{Q_{max} - Q_0}{Q_0} * 100$$	(5)
	ΔQ_{t-1}	magnitude of the preceding storm event	
	RL	relative duration of the rising limb to the duration the storm event (Butturini et al., 2006)	
	k	slope of the initial phase of the recession limb estimated using an exponential model (Singh, 1988)	
	t	duration of the storm event	
	Δt	time from the previous storm event	
	Load	nutrient load calculated from the instantaneous hourly flow *Q(t)* and concentration *C(t)* time series over the storm event duration	

		(t_{start} to t_{end}) $$Load = \int_{t_{start}}^{t_{end}} Q(t)C(t)dt \quad (6)$$
Biogeochemical properties	$\boldsymbol{m}$	mean slope of rising and falling concentration-discharge limbs in log-space. Slope values close to zero indicate chemostatic behaviour as the changes in concentrations are independent of changes in stream discharge (Godsey et al., 2009)
	$\boldsymbol{C_0}$	baseline nutrient concentration prior to the storm event
	$\boldsymbol{C_{max}}$	maximum nutrient concentration during the storm event
	$\boldsymbol{C_{mean}}$	mean nutrient concentration during the storm event
	$\boldsymbol{COND_{mean}}$	mean specific conductivity during the storm event
	$\boldsymbol{pH_{mean}}$	mean pH during the storm event
	$\boldsymbol{DO_{mean}}$	mean dissolved oxygen concentration during the storm event
	$\boldsymbol{RED_{mean}}$	mean redox potential during the storm event
Antecedent conditions	$\boldsymbol{TEMPW_{mean}}$	mean stream water temperature during the storm event
	$\boldsymbol{TEMPA_{mean}}$	mean air temperature during the storm event
	$\boldsymbol{RAD_{mean}}$	mean solar radiation during the storm event
	$\boldsymbol{RAIN_{tot}}$	total amount of rainfall for the event
	$\boldsymbol{RAIN_{int\_mean}}$	average rainfall intensity
	$\boldsymbol{RAIN_{int\_max}}$	maximum rainfall intensity
	$\boldsymbol{\Delta RAIN}$	rainfall duration
	$\boldsymbol{API_7}$	seven day antecedent precipitation
Mean percentage error		mean percentage error. The mean percentage deviation between measured *C(t)* and predicted *Cpred(t)* nutrient concentrations for both optimisation methods, *n* is the number of observations during the storm event $$err = \frac{100}{n}\sum_{1}^{n}\frac{C(t) - C_{pred}(t)}{C(t)} \quad (7)$$

Bowes M, House W, Hodgkinson R, Leach D. Phosphorus-discharge hysteresis during storm events along a river catchment: the River Swale, UK. Water Research 2005: 751-762.

Butturini A, Gallart F, Latron J, Vazquez E, Sabater F. Cross-site comparison of variability of DOC and nitrate c-q hysteresis during the autumn-winter period in three Mediterranean headwater streams: A synthetic approach. Biogeochemistry 2006; 77.

Godsey SE, Kirchner JW, Clow DW. Concentration-discharge relationships reflect chemostatic characteristics of US catchments. Hydrological Processes 2009; 23: 1844-1864.

House WA, Warwick MS. Hysteresis of the solute concentration/discharge relationship in rivers during storms. Water Research 1998; 32: 2279-2290.

Singh VP. Hydrologic Systems: Rainfall-runoff modeling: Prentice Hall, 1988.

Supporting Table B Biogeochemical and meteo-hydrological characteristics of the numbered storm events: *D* - direction of the hysteresis: A – anti-clockwise, Nh – no hysteresis, C – clockwise, C_{mean} – mean concentration, C_{max} – maximum concentration, ΔR – hysteresis area and rotational metric, ΔC – relative concentration change, Q_{mean} – mean discharge, Q_{max} – maximum discharge, API_7 – antecedent precipitation 7 days prior to the event, $TEMPA_{mean}$ – mean air temperature during the event

Storm	**Date**	**TP (µg l^{-1})**					**TRP (µg l^{-1})**					**TURB (NTU)**					**Q_{mean} (m^{3}s^{-1})**	**Q_{max} (m^{3}s^{-1})**	**API_7 (mm)**	**$TEMPA_{mean}$ (°C)**
		D	**C_{mean}**	**C_{max}**	**ΔR (%)**	**ΔC (%)**	***D***	**C_{mean}**	**C_{max}**	**ΔR (%)**	**ΔC (%)**	***D***	**C_{mean}**	**C_{max}**	**ΔR (%)**	**ΔC (%)**				
1	15-16 Jun 09	A	84.6	227.0	-52.4	62.7	A	50.4	89.0	-58.3	43.3	A	1.9	4.0	-54.8	52.5	0.3	0.9	4.8	13.2
2	2-5 Jul 09	A	60.3	125.0	-58.6	54.0	A	45.5	96.0	-54.2	53.2	A	1.1	1.7	-55.7	35.3	0.1	0.4	1.4	16.9
3	24-25 Jul 09	-	-	-		-	A	54.2	71.0	-43.4	23.6	A	1.8	3.2	-47.5	42.8	1.0	1.1	52.0	11.5
4	28-30 Jul 09	C	100.1	126.0	44.1	46.6	C	71.0	125.0	59.3	47.5	C	4.7	10.0	54.4	55.7	6.6	15.0	33.4	11.4
5	1-2 Aug 09	A	41.8	46.0	-72.6	17.3	A	29.8	36.0	-54.9	9.2	A	1.4	1.6	-57.3	14.4	1.0	1.2	30.4	12.1
6	14-16 Aug 09	-	-	-		-	A	32.3	57.0	-47.5	44.3	A	1.3	1.6	-58.9	17.5	0.4	0.5	5.4	13.0
7	26-28 Aug 09	-	-	-		-	Nh	57.1	118.0	0.0	52.0	Nh	3.1	10.1	0.0	70.6	1.8	4.5	20.8	11.8
8	28-29 Aug 09	-	-	-		-	A	36.0	49.0	-41.9	26.6	A	1.5	2.0	-52.7	26.5	1.0	1.1	24.6	11.1
9	29-1 Aug/Sep 09	-	-	-		-	Nh	44.9	144.0	0.0	65.6	C	3.4	22.3	30.8	84.6	4.9	31.4	24.2	11.7
10	24-28 Oct 09	C	33.2	60.0	54.5	37.4	C	32.8	53.0	60.4	45.5	C	1.1	2.5	41.8	57.6	1.0	1.8	15.2	9.1
11	30-1 Oct/Nov 09	Nh	30.5	40.0	0.0	23.9	Nh	27.7	41.0	0.0	32.6	Nh	1.2	2.4	0.0	50.4	1.1	1.7	12.0	9.9
12	1-2 Nov 09	C	69.4	153.0	51.7	54.6	C	73.1	132.0	51.8	44.6	C	7.4	26.1	56.7	71.8	37.8	113.0	20.6	9.1
13	2-3 Nov 09	Nh	56.2	80.0	0.0	26.4	Nh	54.5	74.0	0.0	29.7	Nh	3.2	5.6	0.0	42.9	14.2	29.1	48.2	7.5
14	3-4 Nov 09	Nh	35.6	39.0	0.0	11.3	Nh	30.9	33.0	0.0	7.6	Nh	1.8	2.3	0.0	23.9	4.8	6.3	57.2	7.2
15	12-13 Nov 09	A	46.0	62.0	-33.4	25.8	-	-	-		-	Nh	1.7	3.4	0.0	50.9	2.4	3.9	22.0	6.8
16	13-15 Nov 09	C	61.0	207.0	49.3	70.6	-	-	-		-	C	4.8	27.4	57.5	82.4	25.2	99.5	27.2	8.8
17	15-16 Nov 09	A	51.9	60.0	-59.5	13.5	-	-	-		-	A	2.6	4.2	-58.2	39.1	4.1	4.9	38.2	9.4
18	25-28 Feb 10	C	56.4	147.0	36.5	61.6	C	49.6	92.0	36.3	46.1	C	2.7	14.1	44.1	81.0	1.1	2.1	4.2	1.7
19	20-22 Mar 10	C	34.9	93.0	44.5	62.5	C	27.2	72.0	47.0	62.2	C	2.0	5.7	44.5	65.4	0.6	0.8	3.4	4.6
20	22-23 Mar 10	A	27.1	34.0	-43.0	22.3	A	22.1	28.0	-56.5	20.9	A	1.5	1.9	-50.2	86.6	0.8	0.9	15.4	7.0
21	25-28 Mar 10	-	-	-		-	C	64.9	181.0	32.0	64.1	C	22.2	124.8	50.6	82.2	2.8	7.5	20.6	5.8
22	29-30 Mar 10	A	42.6	82.0	-32.5	48.1	A	43.6	60.0	-20.1	27.3	C	14.5	29.8	27.7	51.5	2.1	3.2	20.2	5.0
23	5-6 Apr 10	Nh	25.0	41.0	0.0	39.2	C	28.9	39.0	59.6	25.8	A	1.5	2.9	-25.2	47.2	1.7	2.4	37.2	5.6
24	6-8 Apr 10	A	29.2	40.0	-55.5	27.0	A	23.7	35.0	-63.2	32.2	A	1.1	1.8	-43.7	39.4	1.5	1.9	30.2	6.1
25	7-9 Jun 10	A	44.9	75.0	-72.5	40.1	A	33.1	56.0	-55.1	40.9	A	2.8	5.4	-67.8	48.9	0.1	0.3	7.2	12.9
26	10-12 Jun 10	A	50.1	75.0	-53.8	33.2	A	46.2	75.0	-65.5	38.4	A	1.8	2.8	-51.0	35.0	0.1	0.2	13.6	11.8
27	13-15 Jun 10	A	40.0	52.0	-61.0	23.2	A	37.7	56.0	-58.6	32.6	A	1.8	3.4	-48.9	47.1	0.1	0.2	15.2	12.3
28	20-23 Jun 10	A	81.4	172.0	-57.9	48.3	A	59.4	115.0	-59.1	52.7	A	0.9	1.1	-47.5	22.7	0.2	0.4	10.6	14.4
29	23-27 Aug 10	A	93.1	142.0	-55.1	46.6	A	52.5	99.0	-45.6	45.0	A	1.8	3.8	-51.6	51.3	0.2	0.2	13.0	11.9
30	2-8 Sep 10	A	31.9	83.0	-56.6	54.7	A	41.7	60.0	-59.9	33.9	-	-	-		-	0.1	0.2	12.8	13.2
31	19-22 Sep 10	A	80.5	124.0	-54.5	41.8	A	65.7	113.0	-48.8	35.0	-	-	-		-	0.2	0.2	18.6	12.2
32	29-1 Sep/Oct 10	C	123.4	204.0	42.8	35.9	C	94.0	137.0	50.7	43.2	C	1.3	1.9	43.7	35.3	0.5	0.6	15.8	9.7
33	1-3 Oct 10	C	108.3	292.0	42.8	62.9	C	84.4	229.0	49.8	63.2	C	3.1	9.9	34.8	69.2	1.2	2.2	11.4	9.1

34	2-5 Oct 10	C	73.4	165.0	43.8	55.5	C	75.7	145.0	50.3	47.8	Nh	1.6	2.9	0.0	43.8	1.1	1.5	20.0	10.3
35	6-9 Oct 10	Nh	68.3	126.0	0.0	44.9	Nh	73.0	117.0	0.0	37.2	Nh	1.3	3.4	0.0	60.3	0.9	1.2	26.8	10.5
36	22-25 Oct 10	C	155.0	884.0	51.9	85.0	Nh	94.9	410.0	0.0	76.3	C	2.3	8.5	41.1	76.7	0.7	1.5	10.4	3.3
37	26-27 Oct 10	Nh	79.9	125.0	0.0	41.9	C/Nh	72.7	125.0	0.0	36.1	C	1.0	1.2	83.6	19.2	0.6	0.6	19.0	9.8
38	27-29 Oct 10	A	90.6	130.0	-48.2	30.3	A	80.6	104.0	-55.5	22.5	A	2.4	4.7	-37.4	49.8	1.4	2.0	24.4	8.5
39	29-31 Oct 10	C	89.2	140.0	52.9	36.3	C	74.9	111.0	58.4	32.5	C	2.4	5.9	22.6	60.9	2.0	3.3	26.6	8.8
40	8-9 Nov 10	C	60.3	134.0	39.2	55.0	C	58.3	125.0	51.1	53.3	C	1.8	3.5	38.5	47.7	2.1	2.8	56.4	4.5
41	9-10 Nov 10	C	50.2	71.0	54.9	29.3	C	50.3	58.0	71.4	13.2	C/Nh	1.3	1.5	72.3	14.7	2.0	2.3	60.4	4.3
42	11-13 Nov 10	-	-	-		-	A/Nh	58.2	110.0	-57.6	47.1	C/Nh	3.8	12.9	37.9	70.3	10.4	41.8	41.2	5.4
43	13-15 Nov 10	Nh	60.0	123.0	0.0	50.7	Nh	51.4	105.0	0.0	51.1	Nh	1.5	4.7	0.0	67.5	2.3	2.8	32.4	5.2
44	18-20 Nov 10	A/Nh	59.6	72.0	-51.6	19.5	Nh	40.3	50.0	-60.0	17.2	Nh	1.2	1.4	-58.9	13.6	1.1	1.1	19.6	4.5
45	2-3 Feb 11	A	81.5	126.0	-46.0	35.3	A	71.5	100.0	-56.6	28.6	A	2.1	4.9	-29.6	58.2	1.2	2.0	1.2	5.5
46	3-4 Feb 11	C/Nh	155.8	298.0	48.3	47.7	C	101.5	180.0	67.6	40.3	C	13.3	40.1	49.8	66.8	27.4	66.4	0.2	6.8
47	4-6 Feb 11	C	115.8	234.0	68.5	53.3	C	62.3	107.0	55.1	63.2	C	7.2	35.2	60.4	79.7	24.1	68.9	0.2	7.1
48	6-7 Feb 11	C	89.1	145.0	41.6	41.6	A	45.3	65.0	-34.8	38.3	C	5.1	15.9	40.5	67.9	20.8	48.6	2.6	6.8
49	6-9 Feb 11	C	103.6	180.0	30.8	49.8	C	47.6	65.0	49.6	37.3	C	5.2	19.3	39.7	73.0	24.6	99.1	4.6	4.2
50	15-17 Feb 11	Nh	53.6	111.0	0.0	52.4	Nh	41.5	58.0	0.0	28.9	Nh	2.2	6.9	0.0	68.6	2.8	3.4	15.0	3.4
51	25-27 Feb 11	C	41.9	73.0	48.9	45.3	C	44.3	66.0	50.5	35.4	C	1.5	3.6	33.7	59.7	1.2	1.6	0.0	5.1
52	9-11 Mar 11	C	41.1	65.0	67.8	36.8	C	37.1	58.0	67.3	36.1	C	1.1	2.2	64.0	50.5	0.6	0.8	9.6	5.3
53	11-14 Mar 11	C	52.4	95.0	62.0	44.9	C	35.8	52.0	70.1	31.1	C	2.4	8.2	56.8	71.2	2.2	3.6	7.2	4.4
54	7-10 May 11	Nh	45.0	116.0	0.0	61.2	A	47.1	85.0	-57.0	44.6	Nh	1.3	4.4	0.0	70.9	0.3	0.7	9.6	12.2
55	21-23 May 11	Nh	59.7	115.0	0.0	48.1	Nh	47.9	102.0	0.0	53.0	Nh	1.3	2.3	0.0	45.2	0.5	0.8	13.2	9.7
56	23-25 May 11	C	87.9	352.0	40.1	77.4	C	48.2	100.0	55.1	53.0	C	3.6	36.6	41.6	90.7	2.7	14.5	24.8	9.0
57	26-30 May 11	C	46.8	169.0	43.9	72.2	C	40.4	168.0	49.1	76.1	C	1.1	3.0	37.4	63.0	1.0	1.6	34.8	9.8
58	18-19 Jun 11	A	83.1	313.0	-54.7	66.5	A	81.8	296.0	-52.9	74.5	A	1.6	3.3	-52.7	56.7	0.2	0.2	10.0	11.8
59	17-18 Jul 11	A	162.9	408.0	-58.5	76.2	A	71.0	298.0	-65.4	60.1	A	1.6	3.3	-62.6	52.4	0.2	0.2	16.8	15.0
60	18 Jul 11	A	180.6	322.0	-73.5	54.1	A	91.4	199.0	-76.1	43.9	A	1.8	2.3	-73.9	23.0	0.2	0.3	30.0	14.2
61	20-21 Jul 11	A	140.7	192.0	-51.0	31.8	Nh	51.1	75.0	0.0	26.7	Nh	1.3	2.1	0.0	36.2	0.3	0.4	47.4	12.5

Supporting Table C Additional biogeochemical and meteo-hydrological characteristics of the numbered storm events: m –slope of the hysteresis, t – duration of the storm event, Δt – time from the previous storm event, Q_{vol} – discharge volume, ΔQ_t – storm event magnitude, ΔQ_{t-1} – previous storm event magnitude, RL – duration of the rising limb, k – slope of the falling limb, Q_0 - baseline discharge prior to the storm event, $\Delta RAIN$ – rainfall duration, $RAIN_{tot}$ – total rainfall prior to the event, H_{mean} – mean stage, RAD_{mean} – mean solar radiation, $COND_{mean}$ – mean specific conductivity, DO_{mean} – mean dissolve oxygen concentration during the storm event

Storm	m_{TP}	m_{RP}	m_{TURB}	t (hours)	Δt (hours)	Q_{vol} (10^3*m^3)	ΔQ_t (%)	ΔQ_{t-1} (%)	RL (hours)	k	Q_0 ($m^3 s^{-1}$)	$\Delta RAIN$ (hours)	$RAIN_{tot}$ (mm)	H_{mean} (m)	RAD_{mean} (W m^{-2})	$COND_{mean}$ (µS cm^{-1})	DO_{mean} (%)
1	1.75	1.38	0.97	32	233	39.3	493.3	-	21.2	0.9	0.2	32	5.2	0.64	82.1	410.2	65.3
2	1.19	1.13	0.47	59	401	30.6	300.0	493.3	51.7	0.3	0.1	59	14.6	0.54	110.6	460.8	57.7
3	-	0.75	1.59	24	35	82.7	16.5	300.0	28.0	1.1	0.9	24	8.0	0.66	69.2	461.2	64.1
4	0.51	0.61	0.57	42	45	1018.4	152.5	16.5	25.6	17.4	5.9	42	21.2	1.19	68.7	384.3	63.5
5	-0.02	0.04	-0.05	31	81	116.0	13.7	152.5	34.4	1.2	1.0	31	4.6	0.67	73.4	459.5	72.1
6	-	1.37	0.21	50	240	65.7	130.4	13.7	58.8	0.5	0.2	50	8.4	0.59	80.2	466.8	61.7
7	-	0.77	1.22	48	76	311.5	637.7	130.4	22.4	4.8	0.6	48	9.8	0.89	71.2	427.3	64.7
8	-	1.39	1.41	28	70	101.0	4.8	637.7	24.1	1.1	1.0	28	5.6	0.66	66.0	461.8	65.6
9	-	0.50	0.58	72	91	1285.3	3509.2	4.8	75.3	37.8	0.9	72	15.4	1.43	70.7	431.3	62.2
10	0.14	0.10	0.58	107	188	369.6	820.0	3509.2	41.7	1.9	0.2	107	11.2	0.73	50.3	453.8	60.4
11	0.45	0.66	0.94	36	219	138.2	252.1	820.0	48.6	1.8	0.5	36	11.2	0.72	56.7	451.9	59.9
12	0.28	0.32	0.52	21	69	2956.1	8029.5	252.1	63.6	147.9	1.4	21	0.2	2.04	50.7	336.5	53.5
13	0.39	0.46	0.61	25	41	1281.6	20.9	8029.5	23.1	34.9	24.1	25	39.4	1.41	38.3	336.5	58.8
14	0.34	0.32	0.73	17	43	297.3	16.0	20.9	27.8	6.7	5.4	17	5.8	0.96	35.8	387.6	62.2
15	0.38	-	1.15	26	77	225.3	163.7	16.0	66.7	4.0	1.5	26	7.0	0.86	32.9	413.4	81.0
16	0.37	-	0.64	44	17	4065.4	340.5	163.7	17.8	124.9	22.6	44	23.8	1.96	48.1	308.9	23.3
17	-0.37	-	0.80	16	56	238.8	5.8	340.5	23.5	5.1	4.7	16	1.6	0.91	52.8	413.2	1.5
18	0.61	0.62	1.08	57	500	232.8	464.9	5.8	48.3	2.2	0.4	57	0.0	0.75	-5.9	636.1	97.5
19	1.53	1.41	1.01	46	538	94.8	207.7	464.9	34.0	0.8	0.3	46	11.2	0.62	16.0	568.3	71.0
20	0.74	0.73	0.82	43	47	117.5	61.4	207.7	40.9	0.9	0.6	43	2.6	0.64	19.1	545.6	72.0
21	-	0.86	1.33	67	76	673.1	396.0	61.4	22.1	7.3	1.5	67	13.0	1.00	25.3	411.6	67.8
22	1.12	0.56	1.41	21	118	159.1	219.0	396.0	54.5	3.4	1.0	21	6.0	0.82	12.8	417.5	69.4
23	0.94	0.30	1.52	27	156	162.8	86.8	219.0	28.6	2.6	1.3	27	3.0	0.77	23.9	398.9	78.5
24	0.81	0.50	1.55	33	50	175.7	32.0	86.8	20.6	1.9	1.5	33	5.0	0.74	28.0	416.4	77.1
25	0.40	0.38	0.53	61	775	23.6	225.0	32.0	27.4	0.2	0.1	61	8.6	0.51	80.0	447.4	40.3
26	0.45	0.44	0.03	59	75	21.6	33.3	225.0	11.7	-	0.1	59	5.0	0.48	71.2	482.7	48.2
27	0.12	0.11	-0.01	42	78	15.6	87.5	33.3	32.6	0.1	0.1	42	8.6	0.47	75.0	479.3	50.2
28	1.12	0.88	0.27	78	758	62.3	600.0	87.5	26.6	0.4	0.1	78	7.6	0.55	91.5	427.4	74.3
29	0.94	1.30	-	92	112	49.8	64.3	600.0	12.9	0.2	0.1	92	11.6	0.50	71.8	446.8	77.1
30	-	0.41	-	35	375	12.9	25.0	64.3	11.1	0.2	0.1	35	9.2	0.47	82.4	445.9	65.0
31	1.99	1.35	-	81	125	43.8	50.0	25.0	43.9	0.2	0.1	81	16.2	0.49	74.3	487.4	65.6

32	1.06	1.04	0.60	51	142	82.9	126.9	50.0	34.6	0.6	0.3	51	9.6	0.59	55.4	453.2	72.2
33	0.81	0.16	1.51	44	52	183.8	347.9	126.9	26.7	2.3	0.5	44	8.4	0.76	50.7	413.9	76.6
34	1.06	0.33	1.49	47	70	184.2	75.6	347.9	27.1	1.5	0.9	47	8.0	0.70	59.6	423.5	79.2
35	1.09	0.21	1.14	81	93	270.5	53.2	75.6	15.9	1.2	0.8	81	10.6	0.67	61.6	434.8	77.6
36	1.97	1.33	2.12	71	400	188.2	694.7	53.2	16.7	1.6	0.2	71	11.2	0.70	23.8	419.1	66.6
37	0.61	0.37	-0.13	22	101	44.1	37.8	694.7	60.9	-	0.5	22	11.4	0.59	55.8	467.5	58.1
38	0.59	0.12	1.45	27	23	136.9	57.3	37.8	17.9	2.0	1.2	27	3.6	0.74	45.9	395.9	61.2
39	0.92	0.30	1.72	48	46	338.3	117.9	57.3	26.5	3.2	1.5	48	5.8	0.83	48.2	402.9	59.9
40	1.04	0.22	1.81	27	122	202.4	91.0	117.9	39.3	2.8	1.5	27	7.6	0.80	15.2	427.1	62.6
41	0.84	0.25	1.04	28	49	201.2	14.1	91.0	34.5	2.3	2.0	28	3.4	0.76	14.3	405.9	65.7
42	-	0.10	0.71	55	75	2096.1	2763.7	14.1	37.5	50.8	1.5	55	18.2	1.55	22.0	355.1	74.9
43	1.22	0.51	1.27	39	78	326.1	5.2	2763.7	2.5	2.7	2.7	39	5.6	0.80	21.0	395.3	81.6
44	1.20	1.03	1.01	41	129	155.6	1.8	5.2	28.6	1.1	1.1	41	4.6	0.66	15.2	428.6	64.5
45	0.45	0.16	0.90	31	470	132.5	371.4	1.8	37.5	2.0	0.4	31	0.0	0.74	18.0	455.4	79.9
46	0.37	0.28	0.71	17	51	1753.1	314.7	371.4	38.9	86.5	16.0	17	0.0	1.76	40.9	304.1	64.1
47	0.12	0.11	0.53	44	44	3880.2	352.1	314.7	42.2	87.1	15.2	44	2.4	1.77	28.8	276.6	51.3
48	0.27	0.46	0.91	21	74	1618.3	483.3	352.1	45.5	59.1	8.3	21	2.4	1.61	19.3	279.3	51.0
49	0.26	0.27	0.70	51	13	4545.6	467.2	483.3	30.8	123.3	17.5	51	6.0	1.96	16.5	277.0	47.4
50	1.19	0.15	1.65	40	62	401.3	42.3	467.2	43.9	3.5	2.4	40	0.0	0.83	12.0	372.9	87.6
51	1.40	0.23	2.25	42	278	184.0	68.5	42.3	30.2	1.6	0.9	42	3.8	0.71	8.2	415.1	81.8
52	0.53	0.24	0.72	46	283	99.9	100.0	68.5	55.3	0.8	0.4	46	1.0	0.62	-11.8	448.8	94.7
53	0.54	0.16	1.01	59	47	465.0	312.8	100.0	20.0	3.7	0.9	59	0.4	0.84	11.1	370.7	87.7
54	1.04	0.58	1.03	69	798	80.4	188.0	312.8	28.6	0.8	0.3	69	13.0	0.61	53.6	443.8	75.0
55	0.91	0.66	0.41	39	345	75.6	583.3	188.0	52.5	0.8	0.1	39	11.6	0.62	26.5	416.3	67.5
56	0.61	0.27	0.92	55	40	549.3	276.6	583.3	12.5	16.0	3.9	55	13.0	1.18	103.5	354.6	73.5
57	0.92	0.43	1.28	83	95	284.9	79.8	276.6	13.1	1.7	0.9	83	11.4	0.71	41.8	410.2	70.6
58	8.47	7.64	3.59	35	565	25.3	33.3	79.8	30.6	0.2	0.2	35	8.8	0.51	41.7	470.6	66.9
59	1.85	1.40	2.95	17	213	9.7	23.5	33.3	27.8	0.2	0.2	17	9.0	0.50	112.6	490.6	40.7
60	0.93	0.71	0.33	13	22	11.3	17.9	23.5	28.6	0.4	0.3	13	13.2	0.53	127.9	418.0	35.7
61	2.63	1.63	1.82	12	68	13.1	20.0	17.9	30.8	0.4	0.3	12	0.0	0.54	45.6	469.9	39.1

Supporting Table D Kruskal-Wallis analysis of variance between storm event groups (A, Nh, C). *H* – the Chi-square statistic, 2 d.f., *N* – number of observations. Significant *p* values at α = 0.05 in bold

	Variable	**TP**					**TRP**					**TURB**				
		A	**Nh**	**C**	***H***	***p***	**A**	**Nh**	**C**	***H***	***p***	**A**	**Nh**	**C**	***H***	***p***
		***N* = 21**	***N* = 12**	***N* = 21**			***N* = 24**	***N* = 13**	***N* = 21**			***N* = 20**	***N* = 13**	***N* = 26**		
	ΔR (%)	-54.65	0.00	48.20	45.80	**0.00**	-53.95	0.00	54.40	49.68	**0.00**	-51.71	0.00	46.39	50.37	**0.00**
	ΔC (%)	39.64	39.97	52.83	7.09	**0.03**	37.43	41.39	45.79	3.87	0.14	40.95	52.59	63.41	16.57	**0.00**
Hydrological properties	Q_0 ($m^3\ s^{-1}$)	0.68	3.58	4.61	11.25	**0.00**	0.83	3.19	3.48	10.48	**0.01**	0.73	3.28	4.07	9.61	**0.01**
	Q_{mean} ($m^3\ s^{-1}$)	0.81	3.60	8.47	15.27	**0.00**	1.80	2.91	6.86	15.15	**0.00**	0.80	2.71	7.92	17.36	**0.00**
	H_{mean} (m)	0.61	0.87	1.07	16.83	**0.00**	0.68	0.85	1.00	16.58	**0.00**	0.62	0.80	1.09	19.71	**0.00**
	Q_{max} ($m^3\ s^{-1}$)	1.14	8.26	25.05	16.75	**0.00**	4.39	6.97	19.60	16.65	**0.00**	1.06	4.68	24.39	19.80	**0.00**
	Q_{vol} ($m^3 * 10^3$)	82.56	470.37	1068.12	25.28	**0.00**	215.34	386.06	879.17	20.77	**0.00**	84.50	300.42	1060.47	25.30	**0.00**
	ΔQ_t (%)	131.78	368.12	633.56	11.91	**0.00**	251.86	489.37	614.40	4.80	0.09	126.67	171.50	799.55	13.52	**0.00**
	ΔQ_{t-1} (%)	140.91	1236.86	356.75	8.62	**0.01**	175.64	1105.49	360.00	2.72	0.08	180.52	1099.15	333.53	2.65	0.08
	RL (%)	30.97	33.61	32.95	0.37	0.83	31.34	35.03	33.12	0.27	0.77	29.23	32.48	36.46	1.38	0.26
	k ($m^3\ s^{-1}$)	1.22	10.58	31.32	15.51	**0.00**	5.39	8.74	24.45	2.42	**0.05**	1.14	5.26	31.47	6.08	**0.00**
	t (hours)	40.20	41.00	47.80	3.18	0.20	43.10	41.80	48.00	1.53	0.47	40.00	40.00	47.70	2.72	0.26
	Δt (days)	9.19	7.62	5.99	2.35	0.31	9.90	5.61	5.76	1.90	0.16	9.11	6.84	5.70	1.02	0.37
	Load (10^2 kg)	12.70	49.73	331.26	27.02	**0.00**	33.43	78.71	180.88	3.93	**0.03**	0.43	2.35	30.09	7.26	**0.00**
Biogeochemical properties	m	1.27	0.82	0.73	1.70	0.43	1.00	0.63	0.41	6.81	**0.03**	1.01	1.12	1.00	2.20	0.33
	C_o (μg l^{-1} or NTU)	45.72	50.84	67.00	5.51	0.06	43.79	50.75	49.55	0.15	0.93	1.32	1.45	3.60	8.51	**0.01**
	C_{mean} (μg l^{-1} or NTU)	65.01	59.97	86.84	7.02	**0.03**	62.63	62.17	60.03	0.05	0.97	1.68	1.78	4.61	8.78	**0.01**
	C_{max} (μg l^{-1} or NTU)	120.91	96.82	201.45	10.12	**0.01**	112.28	115.33	112.86	1.79	0.41	2.92	4.21	18.16	13.88	**0.00**
	$COND_{mean}$ (μS cm^{-1})	449.20	405.52	398.63	11.21	**0.00**	442.15	417.55	408.24	9.01	**0.01**	449.39	414.44	401.13	11.05	**0.00**
	pH_{mean}	6.50	7.63	5.94	5.62	0.06	6.94	7.61	6.61	6.10	**0.05**	6.84	7.02	6.20	3.45	0.18
	DO_{mean} (%)	59.32	71.06	67.00	2.48	0.29	63.03	65.48	70.46	2.56	0.28	59.75	69.50	66.44	2.38	0.30
	RED_{mean} (mV)	284.40	311.49	194.86	1.48	0.48	273.62	354.26	198.67	6.54	**0.04**	289.25	338.25	196.04	3.53	0.17
	$TEMPW_{mean}$ (°C)	14.85	12.26	11.22	11.79	**0.00**	14.79	13.15	11.13	13.27	**0.00**	14.98	13.30	11.20	14.62	**0.00**
Antecedent conditions	$TEMPA_{mean}$ (°C)	10.65	7.84	7.05	11.58	**0.00**	10.62	8.73	6.92	7.63	**0.00**	10.79	8.91	6.99	8.99	**0.00**
	RAD_{mean} (W m^{-2})	62.05	37.03	34.24	8.41	**0.01**	61.76	43.26	33.87	5.60	**0.01**	64.59	42.91	33.86	7.55	**0.00**
	$RAIN_{tot}$ (mm)	6.94	11.80	7.36	1.54	0.46	7.98	11.00	6.70	1.75	0.18	6.63	10.17	8.38	1.11	0.34
	$RAIN_{int\_mean}$ (mm h^{-1})	0.92	0.84	0.74	0.40	0.82	0.92	0.86	0.68	0.93	0.40	0.88	0.96	0.72	0.74	0.48
	$RAIN_{int\_max}$ (mm h^{-1})	2.45	2.85	2.04	1.02	0.60	2.64	2.68	1.93	1.28	0.28	2.35	2.88	2.16	0.74	0.48
	$\Delta RAIN$ (hours)	9.27	11.90	10.40	0.83	0.66	10.12	12.00	10.52	0.36	0.70	8.85	10.41	11.84	1.38	0.26
	API_7 (mm)	18.32	28.35	17.68	3.00	0.22	17.23	27.22	19.36	1.81	0.17	19.10	27.05	19.01	1.31	0.28

Supporting Table E Kruskal-Wallis analysis of variance between storm events groups - groups comparison (A, Nh, C). *H* – the Chi-square statistic, 1 d.f. Significant *p* values at α = 0.05 in bold

		TP						TRP						TURB					
	Variable	**A – C**		**A – Nh**		**C – Nh**		**A – C**		**A – Nh**		**C – Nh**		**A – C**		**A – Nh**		**C – Nh**	
		H	***p***	***H***	***p***	***H***	***p***	***H***	***p***	***H***	***p***	***H***	***p***	***H***	***p***	***H***	***p***	***H***	***p***
	ΔR (%)	32.27	**0.00**	20.62	**0.00**	20.62	**0.00**	33.51	**0.00**	24.52	**0.00**	23.35	**0.00**	34.13	**0.00**	23.35	**0.00**	24.78	**0.00**
	ΔC (%)	6.19	**0.01**	0.03	0.87	3.35	0.07	4.16	**0.04**	0.34	0.56	0.62	0.43	15.00	**0.00**	3.50	0.06	4.17	**0.04**
Hydrological properties	Q_0 ($m^3 s^{-1}$)	10.05	**0.00**	4.92	**0.03**	0.15	0.70	10.02	**0.00**	3.25	0.07	0.71	0.40	9.10	**0.00**	3.72	**0.05**	0.34	0.56
	Q_{mean} ($m^3 s^{-1}$)	13.24	**0.00**	6.36	**0.01**	1.30	0.25	13.65	**0.00**	5.92	**0.01**	0.84	0.36	15.68	**0.00**	6.67	**0.01**	1.78	0.18
	H_{mean} (m)	15.20	**0.00**	5.86	**0.02**	1.64	0.20	15.08	**0.00**	6.33	**0.01**	0.88	0.35	17.97	**0.00**	7.08	**0.01**	2.23	0.14
	Q_{max} ($m^3 s^{-1}$)	15.19	**0.00**	5.95	**0.01**	1.39	0.24	15.15	**0.00**	6.49	**0.01**	0.71	0.40	18.13	**0.00**	7.16	**0.01**	2.04	0.15
	Q_{vol} ($m^3 * 10^3$)	22.48	**0.00**	8.81	**0.00**	3.06	0.08	19.94	**0.00**	6.74	**0.01**	0.95	0.33	22.97	**0.00**	9.19	**0.00**	2.88	0.09
	ΔQ_t (%)	9.75	**0.00**	0.00	0.97	6.56	**0.01**	4.91	**0.03**	0.13	0.72	1.43	0.23	12.17	**0.00**	0.32	0.57	5.55	**0.02**
	ΔQ_{t-1} (%)	3.78	**0.05**	6.64	**0.01**	2.78	0.10	1.68	0.19	1.15	0.28	0.14	0.71	0.87	0.35	1.36	0.24	0.72	0.40
	RL (%)	0.36	0.55	0.13	0.71	0.01	0.90	0.26	0.61	0.07	0.80	0.00	0.96	2.61	0.11	0.14	0.71	0.34	0.56
	k ($m^3 s^{-1}$)	14.00	**0.00**	6.08	**0.01**	0.61	0.43	13.75	**0.00**	6.91	**0.01**	0.29	0.59	18.24	**0.00**	6.60	**0.01**	2.63	0.10
	t (hours)	2.55	0.11	0.00	0.95	2.78	0.10	1.50	0.47	0.36	0.84	11.24	**0.00**	3.58	0.17	0.64	0.73	3.96	0.14
	Δt (days)	2.36	0.12	0.05	0.82	0.66	0.42	2.15	0.14	0.92	0.34	0.19	0.67	1.34	0.25	0.36	0.55	0.06	0.81
	$Load$ (10^2 kg)	24.30	**0.00**	7.87	**0.01**	4.47	**0.03**	18.78	**0.00**	7.43	**0.01**	0.51	0.48	22.57	**0.00**	7.46	**0.01**	4.04	**0.04**
Biogeochemical properties	m	1.36	0.24	0.11	0.74	0.91	0.34	5.62	**0.02**	0.46	0.50	3.72	**0.05**	0.70	0.40	1.72	0.19	1.07	0.30
	C_o (µg l^{-1} or NTU)	3.70	**0.05**	0.04	0.84	4.13	**0.04**	0.01	0.94	0.13	0.72	0.11	0.74	7.33	**0.01**	0.04	0.84	4.10	**0.04**
	C_{mean} (µg l^{-1} or NTU)	5.29	**0.02**	0.03	0.87	4.47	**0.03**	0.05	0.82	0.02	0.90	0.00	0.97	7.33	**0.01**	0.02	0.90	4.49	**0.03**
	C_{max} (µg l^{-1} or NTU)	6.67	**0.01**	0.00	0.95	7.99	**0.00**	1.47	0.22	0.92	0.34	0.07	0.79	11.72	**0.00**	1.72	0.19	5.70	**0.02**
	$COND_{mean}$ (µS cm^{-1})	9.17	**0.00**	5.95	**0.01**	0.45	0.50	7.91	**0.00**	3.30	0.07	1.14	0.29	9.23	**0.00**	5.74	**0.02**	0.92	0.34
	pH_{mean}	4.44	**0.04**	3.20	0.07	0.20	0.65	5.41	**0.02**	1.36	0.24	1.84	0.18	2.96	0.09	1.84	0.17	0.03	0.86
	DO_{mean} (%)	1.07	0.30	2.51	0.11	0.20	0.65	2.22	0.14	0.04	0.85	1.35	0.25	0.73	0.39	2.59	0.11	0.52	0.47
	RED_{mean} (mV)	0.92	0.34	0.13	0.72	1.10	0.29	1.94	0.16	3.09	0.08	5.43	**0.02**	1.07	0.30	0.96	0.33	3.40	0.07
	$TEMPW_{mean}$ (°C)	10.19	**0.00**	3.97	**0.05**	2.14	0.14	11.31	**0.00**	3.13	0.08	4.39	**0.04**	12.32	**0.00**	2.90	0.09	5.26	**0.02**
Antecedent conditions	$TEMPA_{mean}$ (°C)	10.13	**0.00**	3.50	0.06	2.31	0.13	11.74	**0.00**	3.66	0.06	4.58	0.03	13.48	**0.00**	2.84	0.09	5.16	**0.02**
	RAD_{mean} (W m^{-2})	7.29	**0.01**	3.50	0.06	0.73	0.39	8.54	**0.00**	3.42	0.06	1.62	0.20	10.72	**0.00**	4.39	0.04	1.91	0.17
	$RAIN_{tot}$ (mm)	0.03	0.87	1.34	0.25	1.21	0.27	1.08	0.30	1.15	0.28	1.53	0.22	0.47	0.49	1.48	0.22	0.01	0.92
	$RAIN_{int\_mean}$ (mm h^{-1})	0.36	0.55	0.00	0.98	0.18	0.67	0.90	0.34	0.06	0.81	1.26	0.26	0.15	0.70	1.48	0.22	2.67	0.10
	$RAIN_{int\_max}$ (mm h^{-1})	0.80	0.37	0.01	0.94	0.60	0.44	1.64	0.20	0.09	0.77	2.14	0.14	0.08	0.78	0.32	0.57	0.55	0.46
	$\Delta RAIN$ (hours)	0.52	0.47	0.60	0.44	0.08	0.78	0.05	0.83	0.40	0.53	0.13	0.72	3.32	0.07	0.38	0.54	0.78	0.38
	API_7 (mm)	0.53	0.47	1.59	0.21	2.71	0.10	0.02	0.89	3.54	0.06	2.02	0.15	0.10	0.75	1.82	0.18	2.23	0.14

Supporting Table F Optimisation of the concentration-discharge hysteresis. p_{HW} and p_B - the response factors (positive values indicate clockwise, negative – anti-clockwise hysteresis direction), h – the magnitude factor, g – the gradient constant (House and Warwick, 1998; Bowes et al., 2005)

	Hysteresis direction						Hysteresis magnitude						Mean deviation (%)					
	p_{HW} (mmol m^{-6}s^{2}) [1]			p_B (mmol m^{-6}s^{2}) [2]			h (mmol m^{-3}) [1]			g (mmol s^{-1}) [2]			[1]			[2]		
	TP	TRP	TURB	TP	TRP	TURB	TP	TRP	TURB	TP	TRP	TURB	TP	TRP	TURB	TP	TRP	TURB
1	-0.3	-4.6	0.5	-0.3	-2.9	1.4	4.5	2.6	2.9	0.5	0.3	0.4	-24.8	-17.0	-30.3	-28.7	-22.1	-43.6
2	-12.5	-15.1	-2.6	-7.6	-9.2	-0.9	2.7	3.4	1.6	0.3	0.4	0.2	-9.2	-10.8	-5.4	-25.8	-28.6	-26.6
3	-	-7.9	-8.8	-	-0.1	-0.2	-	3.6	5.8	-	3.1	5.0	-	-0.7	-3.8	-	-1.2	-4.1
4	0.6	0.8	2.3	0.3	0.5	1.5	2.9	2.7	6.3	-118.4	-143.2	-242.0	-24.6	-44.4	-36.5	1115.5	1420.8	1142.3
5	-16.3	-13.8	-28.2	-4.2	-3.6	-3.5	1.7	1.9	1.3	0.3	-0.2	-1.0	6.1	2.7	-2.0	14.4	11.5	7.4
6	-	-40.6	-8.2	-	-12.7	7.3	-	2.3	1.7	-	0.6	0.6	-	-5.8	-0.6	-	-17.7	-24.8
7	-	0.1	1.6	-	0.1	1.2	-	2.7	4.6	-	0.9	1.7	-	-16.9	-41.1	-	13.9	-8.3
8	-	6.5	75.6	-	-3.3	-16.3	-	2.6	2.6	-	1.0	1.3	-	2.8	10.5	-	-4.1	3.7
9	-	0.0	0.8	-	0.0	0.8	-	3.2	7.9	-	-6.9	-5.5	-	4.0	18.5	-	41.8	39.9
10	2.9	4.5	3.3	3.1	4.5	2.8	1.1	1.1	1.3	0.2	0.2	0.3	-5.8	-11.8	-24.8	-4.9	-10.5	-24.6
11	-0.8	-0.4	-1.4	0.4	0.3	-0.3	1.3	1.4	2.1	0.5	0.5	0.9	-2.2	-4.4	-7.5	9.7	5.6	0.6
12	0.0	0.0	0.3	0.2	0.2	0.4	3.0	3.2	11.2	-116.6	-112.7	-98.2	-10.5	-9.6	-38.6	2271.7	1992.4	838.8
13	-0.3	-0.4	-0.6	126.6	136.9	227.9	2.7	2.9	5.0	1532.3	1657.5	2760.9	-3.7	-4.3	1.2	1.1 E+05	1.2 E+05	13048.1
14	0.0	0.1	-0.8	0.1	0.1	-0.1	1.3	1.2	3.2	-335.4	-292.2	-439.7	-3.9	-2.8	1.1	992.5	990.5	798.0
15	-0.5	-	-0.2	-0.2	-	-0.2	2.0	-	3.2	-7.9	-	-3.7	-1.4	-	-12.7	187.0	-	112.8
16	0.1	-	0.5	0.0	-	0.3	2.4	-	6.9	-300.9	-	-337.0	-29.1	-	-100.3	5465.0	-	3906.1
17	13.4	-	3.5	46.9	-	68.5	0.2	-	0.9	116.3	-	197.7	18.7	-	20.1	313.1	-	351.2
18	5.8	1.7	19.5	5.1	2.0	14.3	2.4	2.1	4.0	0.7	0.6	1.2	-18.7	-13.2	-68.8	-14.3	-8.6	-69.6
19	10.4	7.1	26.0	4.8	3.1	12.8	1.8	1.4	2.9	0.4	0.4	0.8	-23.0	-21.3	-24.4	-33.4	-29.2	-38.4
20	-5.1	-5.0	-15.4	2.3	1.7	1.1	1.3	1.2	3.2	1.0	0.9	2.2	-1.9	-0.3	-15.9	-20.0	-17.1	-33.1
21	-	0.9	68.4	-	0.6	48.8	-	3.6	50.8		-5.0	12.0	-	-35.9	-99.2	-	145.2	26.5
22	0.2	-0.1	11.1	0.3	0.3	6.6	2.5	2.0	27.6	0.6	-0.9	12.9	-15.8	-3.6	-17.5	39.3	84.1	21.7
23	-0.2	0.7	-1.6	0.0	0.5	-0.7	1.3	1.2	3.0	-0.1	-0.5	1.2	-8.9	-0.4	-12.5	57.6	74.4	33.2
24	-1.4	3.3	-5.4	-0.3	1.1	-0.8	2.5	1.3	3.1	-1.3	-3.3	-1.9	11.4	0.2	1.0	51.5	58.6	43.8
25	-29.4	-8.3	-40.7	-16.4	-2.3	-24.0	3.1	1.5	5.8	0.3	0.2	0.6	3.0	-4.7	-3.8	-18.6	-43.0	-28.5
26	-68.9	-123.8	-9.5	-69.5	-73.3	-49.6	1.5	2.1	2.0	-0.2	-0.2	-0.3	13.8	-1.1	0.5	-13.0	-32.6	-26.4
27	-38.5	-45.2	1.2	-18.5	-16.5	2.8	2.2	2.3	2.8	0.4	0.3	0.5	3.5	5.0	1.7	-33.9	-28.6	-39.6
28	-47.5	-60.9	-4.1	-32.5	-39.8	-1.2	2.8	3.6	1.0	0.2	0.2	0.1	-16.3	-19.3	-2.0	-21.3	-29.5	-17.2
29	-27.9	-90.9	30.3	-29.4	-51.0	-36.8	3.5	5.3	-2.1	0.5	0.9	-0.3	11.2	-12.6	84.6	10.1	-13.8	81.0
30	-42.9	-41.7	-	-24.4	-12.5	-	1.9	1.8	-	0.3	0.4	-	11.5	-2.4	-	-17.9	-42.2	-
31	-550.4	-478.8	-	-73.4	-41.4	-	5.7	6.0	-	1.1	1.3	-	-4.6	-1.5	-	-39.0	-41.2	-
32	24.3	59.9	17.5	20.4	40.5	14.2	4.8	6.2	1.7	1.4	1.9	0.6	-4.7	-7.1	-4.6	-23.7	-27.6	-31.5
33	9.4	6.5	10.6	6.9	5.4	7.0	4.8	2.9	5.1	1.7	0.9	2.0	-20.4	-4.7	-55.8	-10.7	10.0	-52.4

34	27.2	24.8	7.6	7.0	7.0	2.2	4.4	3.1	3.5	1.9	0.4	1.7	-9.7	-5.9	-11.2	6.9	14.6	4.5
35	-29.4	-17.2	7.8	-9.3	-6.6	2.1	5.2	3.9	3.4	3.6	2.6	2.4	2.2	3.3	-6.7	4.4	6.3	-3.8
36	42.8	20.8	12.7	33.8	16.9	10.2	5.6	3.7	2.5	0.9	0.6	0.4	-55.4	-27.5	-54.4	-63.1	-35.7	-61.5
37	125.0	126.5	17.8	52.0	57.6	21.0	3.1	3.6	0.5	2.8	3.1	0.9	-8.4	-4.1	-4.4	-47.0	-40.6	-52.1
38	-1.9	-1.6	0.3	0.1	0.2	0.8	3.9	2.9	3.9	1.4	0.5	1.9	-5.1	-1.5	-19.2	25.9	40.0	-0.4
39	5.1	2.1	4.4	3.1	1.7	2.1	5.6	3.3	6.2	-15.2	-17.8	-8.1	-4.7	0.2	-20.8	97.1	129.8	67.2
40	8.7	8.6	4.1	1.6	1.1	0.9	3.8	2.3	4.2	-6.6	-13.6	-2.8	-4.7	-4.5	-7.2	113.8	180.1	85.1
41	26.4	14.5	10.1	39.2	42.0	29.4	2.9	1.9	2.5	-44.8	-49.7	-33.9	0.1	-2.6	2.5	68.6	73.8	65.0
42	-	0.0	0.4	-	0.0	0.4	-	2.0	5.4	-	-43.2	-23.5	-	-1.0	-47.2	-	1239.0	493.7
43	-5.5	-2.6	-24.3	30.0	26.0	24.6	2.9	2.4	1.3	89.2	76.1	63.3	2.5	0.1	-0.2	441.5	416.9	434.0
44	65.7	258.3	-28.5	12.1	-6.2	20.1	2.6	2.2	2.4	1.0	0.1	1.0	3.3	9.9	-1.5	1.8	7.5	-2.3
45	0.5	0.9	0.0	1.2	1.6	0.4	3.4	2.6	3.1	1.1	0.7	1.1	-7.0	-2.3	-28.1	4.0	12.3	-19.6
46	0.1	0.1	0.8	0.3	0.2	0.8	5.9	4.4	16.7	-82.6	-89.3	-35.7	-12.2	-8.1	-55.6	1236.1	1654.9	373.5
47	0.1	0.1	0.2	4.6	4.2	7.4	3.6	2.0	10.3	2.1E+04	1.9E+04	3.3E+04	-17.7	-93.2	-26.2	1.9 E+05	2.5 E+04	8602.2
48	0.1	0.0	0.4	-0.6	-0.2	-0.2	3.2	1.9	9.0	4.9E+03	1.5E+03	3.6E+03	-10.1	-6.1	-35.1	1.2 E+04	7978.9	5685.6
49	0.1	0.0	0.5	10.5	7.1	17.0	2.8	2.0	5.1	177.2	123.7	298.1	11.8	-10.3	30.0	532.8	526.8	950.1
50	0.3	0.1	4.3	1.0	1.1	3.0	5.2	2.4	6.0	-26.1	-41.7	-59.6	7.7	6.6	-22.4	168.6	290.7	240.6
51	9.6	10.7	0.0	3.5	3.2	0.3	3.0	1.6	3.8	1.5	-0.7	2.1	-9.8	-5.1	-19.3	14.4	32.6	4.4
52	37.4	39.7	13.1	25.1	25.2	13.3	1.4	1.4	1.6	0.8	0.7	0.8	-11.0	-2.4	-5.4	-37.1	-25.9	-25.1
53	2.4	0.9	11.3	2.0	0.9	7.9	2.1	1.2	3.3	0.0	-0.4	1.1	-8.6	-2.3	-31.5	71.6	102.2	23.5
54	-8.2	-9.4	3.9	-5.5	-6.3	2.2	3.9	3.0	2.9	0.9	0.8	0.8	9.6	7.7	-11.2	4.9	-2.1	-23.0
55	-6.1	-3.0	0.2	-4.9	-2.1	0.8	2.8	2.1	1.6	0.3	0.2	0.2	-28.9	-14.6	-7.2	-30.7	-18.1	-13.7
56	0.2	0.1	0.7	0.2	0.1	0.7	3.8	1.7	6.7	-1.6	-2.0	1.9	-47.5	-13.0	-143.4	109.2	161.2	-27.6
57	36.3	39.0	13.2	11.7	12.8	4.4	4.4	3.3	3.1	2.7	1.8	1.6	14.5	10.6	-7.4	22.5	20.8	1.3
58	-1222.0	-922.2	-227.7	-244.8	-166.6	-27.2	19.7	13.5	3.9	3.6	2.7	1.4	-54.0	-26.4	-15.7	-42.5	-40.2	-65.0
59	-590.5	-846.0	-182.1	-128.7	-190.6	-38.7	12.3	20.1	4.5	1.8	3.5	1.0	17.4	15.1	4.0	15.6	3.6	-16.1
60	-233.2	-356.8	-48.8	-60.5	-83.7	-12.6	10.7	17.2	4.2	2.4	4.6	1.2	53.0	35.4	32.5	88.9	36.3	29.4
61	-49.6	-77.4	-17.7	-8.8	-3.2	0.0	5.0	10.1	3.0	1.3	3.3	1.0	0.6	-1.2	-3.1	-12.4	-33.2	-35.1

[1] House and Warwick, 1998

[2] Bowes et al., 2005

Supporting Table G Results of redundancy analysis with forward selection showing contribution of each variable independently (conditional effects, *Var* – proportion of variance in the response matrix explained by the variable) and Pearson's correlations with the site scores of the first two canonical axes of the full model (R_{axis1} and R_{axis2}). Significant correlations in bold (at α= 0.05 level)

Variable	TP					TRP					TURB				
	F	p	Var	R_{axis1}	R_{axis2}	F	p	Var	R_{axis1}	R_{axis2}	F	p	Var	R_{axis1}	R_{axis2}
Q_{vol}	15.67	0.00	0.34	**0.64**	-0.09	6.41	0.00	0.15	**0.45**	0.16	12.09	0.00	0.29	**0.60**	0.10
DO_{mean}	13.81	0.00	0.31	**0.62**	-0.10	10.66	0.00	0.22	**0.55**	-0.18	10.52	0.00	0.27	**0.57**	0.05
pH_{mean}	10.39	0.00	0.25	**0.56**	-0.11	9.17	0.01	0.20	**0.52**	-0.09	11.77	0.00	0.29	**0.59**	0.09
$TEMPA_{mean}$	10.31	0.00	0.25	**-0.54**	**0.35**	12.68	0.00	0.26	**-0.58**	**0.39**	9.40	0.00	0.24	**-0.55**	-0.02
$TEMPW_{mean}$	10.26	0.00	0.25	**-0.54**	**0.34**	12.37	0.00	0.25	**-0.57**	**0.39**	9.39	0.00	0.24	**-0.54**	-0.02
RAD_{mean}	8.58	0.01	0.22	**-0.50**	**0.42**	10.08	0.01	0.21	**-0.53**	**0.33**	8.42	0.00	0.22	**-0.52**	0.11
ΔQ_t	4.29	0.02	0.12	**0.39**	0.04	1.28	0.28	0.03	0.18	**0.34**	3.89	0.05	0.12	**0.38**	-0.03
Q_{max}	4.00	0.02	0.11	**0.37**	0.06	1.93	0.17	0.05	**0.25**	0.19	4.24	0.01	0.13	**0.39**	0.15
k	3.85	0.04	0.11	**0.37**	0.07	1.64	0.26	0.04	**0.23**	0.20	4.11	0.01	0.12	**0.38**	0.15
Q_{mean}	3.84	0.05	0.11	**0.35**	**-0.32**	4.41	0.03	0.11	**0.38**	-0.20	2.91	0.09	0.09	**0.33**	-0.16
C_{max}	2.92	0.08	0.09	0.16	**0.81**	1.99	0.20	0.05	-0.11	**0.67**	0.68	0.39	0.02	0.10	**0.37**
ΔQ_{t-1}	2.70	0.03	0.08	**0.31**	-0.12	2.38	0.07	0.06	**0.29**	-0.04	1.79	0.12	0.06	**0.27**	0.00
API_7	1.72	0.20	0.05	**-0.24**	**-0.27**	0.74	0.39	0.02	-0.10	**-0.36**	1.73	0.24	0.06	**-0.22**	**-0.38**
C_{mean}	1.59	0.21	0.05	0.16	**0.53**	1.63	0.19	0.04	**-0.21**	**0.32**	0.96	0.46	0.03	0.20	0.02
RED_{mean}	1.56	0.26	0.05	**-0.24**	0.10	2.26	0.10	0.06	**-0.28**	0.16	1.99	0.16	0.06	**-0.28**	0.06
C_0	1.29	0.29	0.04	0.09	**0.57**	1.59	0.19	0.04	**-0.21**	**0.31**	0.93	0.51	0.03	0.19	0.02
Q_0	1.10	0.41	0.03	0.19	**-0.24**	2.05	0.21	0.05	**0.23**	**-0.40**	0.57	0.61	0.02	0.15	-0.12
$RAIN_{tot}$	0.78	0.30	0.02	-0.11	**0.39**	1.99	0.20	0.05	-0.15	**0.61**	0.36	0.55	0.01	-0.12	0.10
RL	0.64	0.46	0.02	0.11	**-0.32**	0.07	0.92	0.00	0.05	-0.04	1.15	0.29	0.04	**0.21**	-0.18
Δt	0.50	0.54	0.02	-0.08	**0.33**	1.42	0.28	0.04	-0.18	**0.37**	0.19	0.76	0.01	-0.07	0.16
$COND_{mean}$	0.30	0.73	0.01	-0.11	0.06	1.08	0.21	0.03	-0.19	0.11	0.24	0.71	0.01	-0.02	0.28
$RAIN_{nt\ mean}$	0.64	0.46	0.02	-0.09	**0.38**	0.76	0.45	0.02	-0.12	**0.29**	0.12	0.84	0.00	-0.05	0.12
$RAIN_{int\_max}$	2.00	0.09	0.06	**-0.25**	**0.33**	4.07	0.04	0.10	**-0.34**	**0.36**	1.11	0.31	0.04	-0.20	0.15
$\Delta RAIN$	0.07	0.86	0.00	0.03	0.12	0.59	0.42	0.02	-0.01	**0.41**	0.23	0.66	0.00	0.09	-0.09

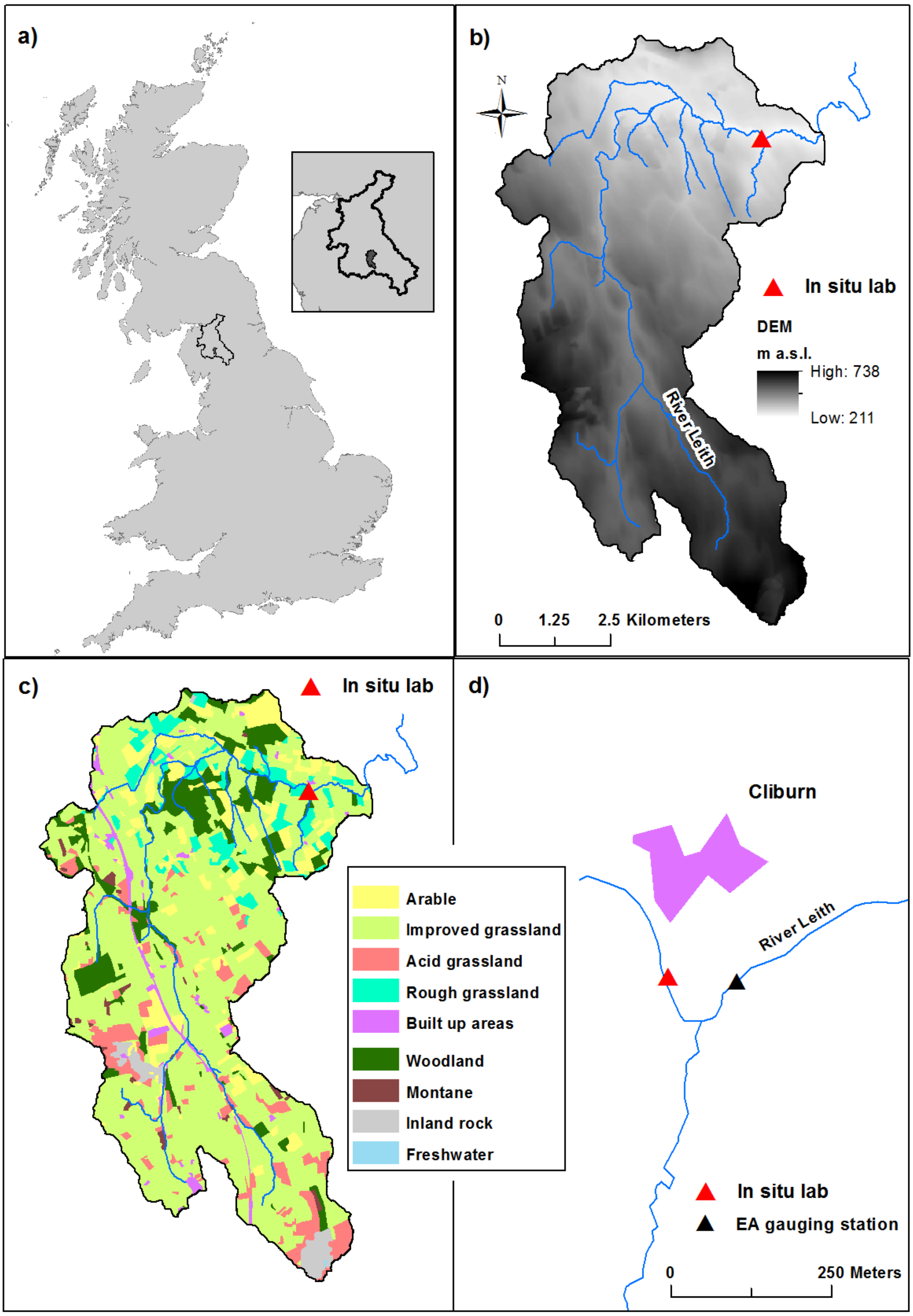

Supporting Figure A Map showing a) location of the River Eden and the River Leith catchments, b) Digital Elevation Model of the River Leith catchment (NEXTMap, 2011), c) Land cover map of the River Leith catchment (LCM2007, 2011) and d) a location of the *in situ* nutrient monitoring and Environment Agency gauging station

LCM2007. Land cover map 2007. Raster data - Great Britain. 2011.
NEXTMap. NEXTMap British Digital Terrain Model Dataset. 2011.

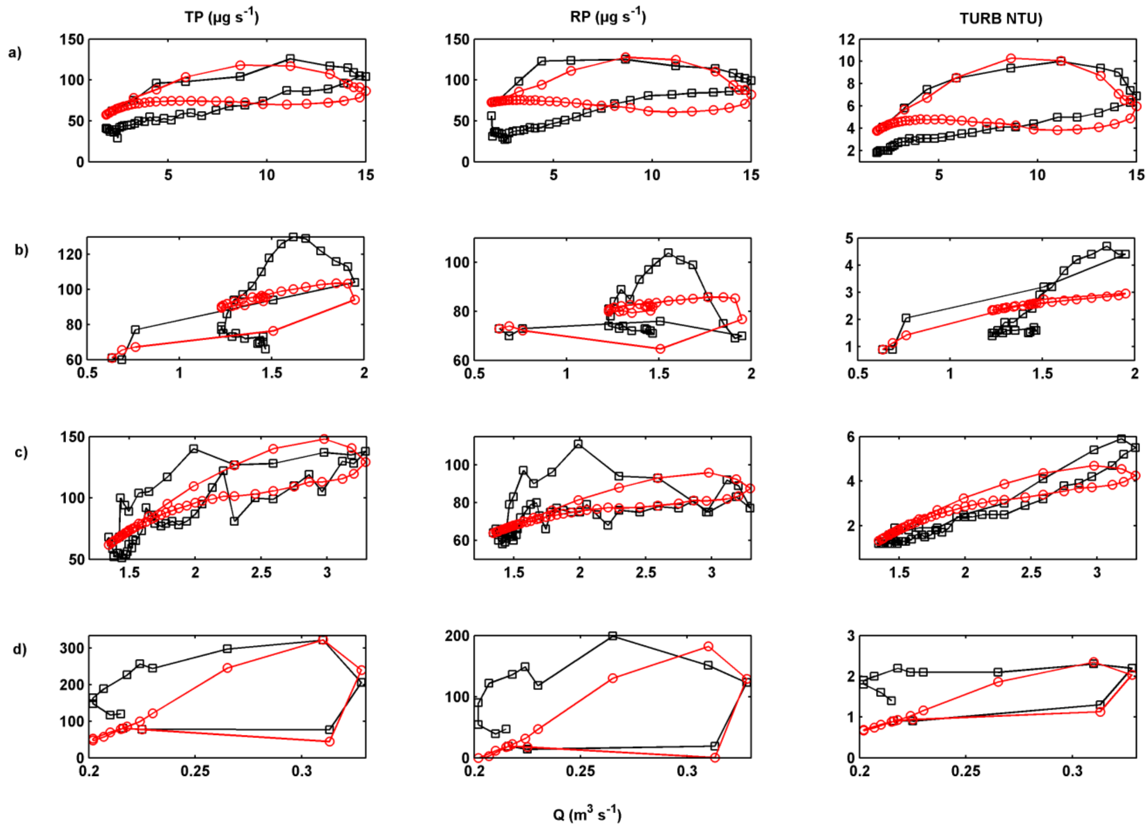

Supporting Figure B Observed (black squares) vs. optimised (red circles) hysteresis loops for selected storm events a) 28-30 July 2009, b) 27-29 October 2010, c) 29-31 October 2010, d) 18 July 2011. TP, TRP and TURB concentrations on the y-axes, discharge on the x-axis

Supplementary Text A OPTIMISATION OF THE HYSTERESIS LOOPS

Two hysteresis optimisation methods, frequently used in high-frequency nutrient analysis provided a quantitative description of the magnitude and direction of the *c*-*q* hysteresis patterns (Supporting Table F). All optimisation parameters showed similar range and mean values for all determinands but varied between the two methods e.g. TP mean *pHW* = -46.9 and pB = -5.2 and the greater range of *pHW* (-1222-125) compared to the *pB* (-245-127mmol $m^{-6}s^{2}$). The storm events with the lowest values of *pHW* (26, 31, 58, 59 and 60) showed large differences between rising and falling limb concentrations producing large, open and round hysteresis loops. The response factors *pHW* and *pB* were significantly correlated for all determinands e.g. TP Spearman's rho $\rho = 0.86$ ($N = 54$, $p = 0.05$) but there was a poorer agreement between the magnitude parameters *h* and *g*. A direct comparison between the magnitude h and gradient g factors was less feasible as both terms have different units (mmol m^{-3} and mmol s^{-1} respectively) and *h* values are constrained ($h > 0$). Nevertheless the mean values of both parameters showed a similar pattern with the highest values for TURB and similar values for both TP and TRP (Supporting Table F).

Optimisation results presented here showed a much wider range for all determinands compared to those reported by authors of each method (Bowes *et al*., 2005; House and Warwick, 1998) as a result of a greater number of storm events analysed in our study (61 compared to 3 in House and Warwick, 1998 and 10 in Bowes *et al*., 2005) and a greater variation of *c*-*q* responses including a high number of anti-clockwise events (24 for TRP compared to 8 for Bowes *et al.*, 2005).

The rotational parameter *pB* did not yield any significant consistent correlations unlike *pHW* which indicated flow discharge and mean temperature as the main controls of hysteresis direction. From the two optimisation methods reported here, only the House and Warwick

(1998) method produced acceptable results in terms of low values of mean percentage deviation between observed and optimised concentrations and agreement between actual and modelled direction of the hysteretic loops. Bowes *et al*. (2005) suggested that their results based on every 3-hour sampling are biased towards more measurements on the falling limb compared to the rising limb (shorter duration). They also noted that their optimisation approach is prone to produce higher errors if the hysteresis patterns do not follow a simple loop pattern, which is in agreement with our results. We observed large errors in the hysteresis optimisation for complex c-q responses (Supporting Figure B and Table 4): (a) multiple peaks (storms 1, 45, 48), (b) open-type hysteresis when $Q_0 \sim= Q_{end}$ e.g. for storm events in series (storms 8, 17, 20, 22, 38, 44, 45), (c) concentration data with a high degree of variation (27, 29, 44, 48) and near the minimum level of detection (8, 20, 24, 49). High-frequency data presented here show that c-q responses rarely follow a simple loop pattern and often exhibit several concentration peaks and different behaviours at different stages of the hydrograph.